Task 1.2

Task Title

Reservoir Modelling and Validation

Research Partners

Swiss Federal Institute of Technology in Zurich (ETHZ), École Polytechnique Fédérale de Lausanne (EPFL), University of Lausanne, University of Geneva, University of Neuchâtel, University of Bern, Università della Svizzera Italiana (USI), Paul Scherrer Institute (PSI), University of Applied Sciences Rapperswil (HSR), Swiss Seismological Service (SED)

Current Projects (presented on the following pages)

Hydraulic stimulation and THM processes, experiments, code development, modelling (collaboration with tasks 1.3 and 4.3)

Fully Hydro-Mechanically coupled Response of Fluid Injection in Rough Fractures on Laboratory and Reservoir Scale: Experiments and Simulations
D. Vogler, R. R. Settgast, C. Annavarapu, C. Madonna, P. Bayer, F. Amann

Fluid injection in a frictional weakening fracture. Nucleation and arrest of dynamic instability
F. Ciardo, B. Lecampion

The tip region of a hydraulic fracture driven by a power law fluid
F.-E. Moukhtari, B. Lecampion

Finite element modeling of three-dimensional fracture growth using unstructured tetrahedral meshes
M. Nejati, T. Driesner

Characterization of the in-situ stress field at Grimsel Test Site
H. Krietsch, N. Dutler, V. Gischig, K. Evans, B. Valley, F. Amann

A slip induced stress transfer model for embedded discrete fractures
G. Jansen, S. A. Miller

Physical Rock Properties Relevant for Deep Geothermal Projects
P. Hardegger, H. R. Schneider, R. Schnellmann

Investigation of chemical stimulation of geothermal reservoirs using reactive flow-through system
J. Ma, X. Z. Kong, M. O. Saar

Long-term reservoir operation and optimization, exploration and reservoir characterization (collaboration with task 1.1 and 4.3)

Numerical simulation of the feasibility of ultra-deep, single-well geothermal power production
T. Driesner

Numerical simulation of CO2 injection into the Upper Muschelkalk aquifer, N. Switzerland: insights into fluid–rock reactions in the aquifer and at the contact to an overlying clay formation
P. Alt-Epping, L. W. Diamond

Towards modeling geochemical effects on long-term permeability evolution and heat extraction
J. Mindel, T. Driesner

Development of efficient numerical methods and codes for geochemical modeling and reactive transport calculations with applications in geothermal energy and carbon sequestration in geological formations
P. Schaedle, A. M. M. Leal , A. Ebigbo, N. Garapati, M. O. Saar

Hydromechanical aspects of CO2 breakthrough and flow in clay-rich caprock
R. Makhnenko, D. Mylnikov, V. Vilarrasa, L. Laloui

The effect of pressure on CaSO4 solubility in geothermal systems
D. Zezin

Numerical modeling of seismic velocity dispersion and attenuation in 3D fractured media
J. Hunziker, B. Quintal, E. Caspari, C. Mallet, G. Rubino, K. Holliger

Numerical Modeling of Natural Convection in Fractured Media
J. Patterson, T. Driesner

International collaborations on integrated geothermal systems characterization (COTHERM = SNF Sinergia project, ETHZ, PSI, University of Iceland)

Dynamics of boiling and condensation of saline fluids above magmatic intrusions
S. Scott, T. Driesner, P. Weis

Reactive transport modelling of two-phase geothermal systems
A.Yapparova, D.A.Kulik, T.Driesner

COTHERM – Seismic Characterization of Fractured Magmatic Geothermal Reservoirs
M. Grab, H. Maurer, S. Greenhalgh

Task Objectives

Task 1.2 focuses on reservoir modelling and validation to address fundamental challenges in DGE:

- Work towards a quantitative understanding and prediction of the fundamental, interacting thermos-hydro-mechanical (THM) processes during hydraulic stimulation. Experimental rock mechanical studies, cross-involvement in deep underground laboratory experiments (Task 1.3), and development of cutting edge numerical tools (in close collaboration with Task 4.3) are the key approaches. Also, alternative stimulation methods are investigated.
- Predict the long-term evolution and optimum efficiency of reservoirs during operation (e.g., efficient and sustainable heat production from fractured reservoirs) for both deep geothermal and CO2 reservoirs, in collaboration with Tasks 1.1, 1.3, 4.3
- Utilize international collaborations with “established” geothermal countries (US, Iceland, New Zealand) to test and optimize methods and to gain experience in applying them to actual, operating systems.

Interaction Between the Partners – Synthesis

- NRP70 collaboration between ETHZ, UNiNE and USI: regular interactions and meetings, joint strategic discussions on code development
- Various interactions on meetings, workshops etc. held by related projects (GEOTHERM-2, NRP70, COTHERM)
- Swiss Geoscience Meeting Session in Deep Geo Energies
- Mutual direct involvement of staff of different partners in various projects and across tasks (e.g., NRP70 project that involves UniBE, UniL, ETHZ and links across tasks 1.1 and 1.2; NRP70 project that involves ETHZ, UniNE, USI and links tasks 1.2 & 4.3, GEOTHERM-2 involves and links across tasks ETHZ, PSI, EPFL, UniBE, UniNE)
- Numerous bilateral and trilateral discussions regarding new simulation code developments, including coding “bootcamp”

Highlights 2016

- Task 1.2 has heavily strengthened expertise in the field of fracture mechanics related to hydraulic stimulation and first results are incoming (e.g., posters by Vogler, Ciardo, Moukhtari, Nejati)
- First simulations of fluid flow and heat transfer in nominally impermeable fractured media (Patterson)
- Predictions on long-term effects in CO2 storage formations (Alt-Epping, Makhnenko)
- Characterisation of stress field at Grimsel Test Site forms essential basis for the coming stimulation experiment (Krietsch, compare also posters of Task 1.3)

SCCER SoE

SWISS COMPETENCE CENTER for ENERGY RESEARCH
SUPPLY of ELECTRICITY

GEL Geothermal Energy & Geofluids

SCCER-SoE Annual Conference 2016

In cooperation with the CTI

Energy
Swiss Competence Centers for Energy Research

Schweizerische Eidgenossenschaft
Confédération suisse
Confederazione Svizzera
Confederaziun svizra

Swiss Confederation

Commission for Technology and Innovation CTI

Fully Hydro-Mechanically coupled Response of Fluid Injection in Rough Fractures on Laboratory and Reservoir Scale: Experiments and Simulations

D. Vogler [1] R.R. Settgast [2] C. Annavarapu [2] C. Madonna [1] P. Bayer [1] F. Amann [1]

ETH zürich [1]ETH Zurich, Zurich, Switzerland [2]Lawrence Livermore National Laboratory, Livermore, USA Lawrence Livermore National Laboratory

Introduction

- Geothermal reservoirs rely on sufficiently high fluid production rates.
- Hydro-Mechanically coupled processes can lead to non-linear fracture opening/closure or injection pressure behavior.
- These phenomena are complicated by heterogeneous fractures.
- This work investigates:
  1. Fracture closure, coupled fluid injection pressure and contact stress behavior in laboratory experiments.
  2. Simulation of performed experiments.
  3. Simulation of fluid injection in reservoir system.

Hydro-mechanically coupled laboratory scale experiments

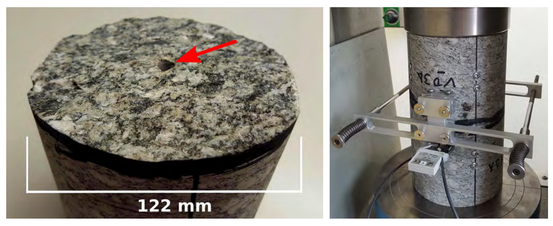

Figure : Experimental setup.

Axial loading (0.25-10 MPa)

i Mechanical fracture behavior.
ii Contact stresses.
iii HM effects.

- Extended GEOS (LLNL) framework for heterogeneous HM processes
- Local cubic law
- Local a_{mech} and a_{hyd}

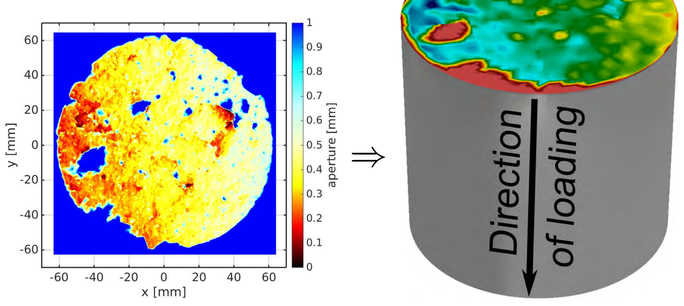

Figure : Aperture measurement used as model input.

Simulating laboratory tests

Stress distribution, fracture contact stresses and fracture closure are modeled for the axial loads applied in the experiments.

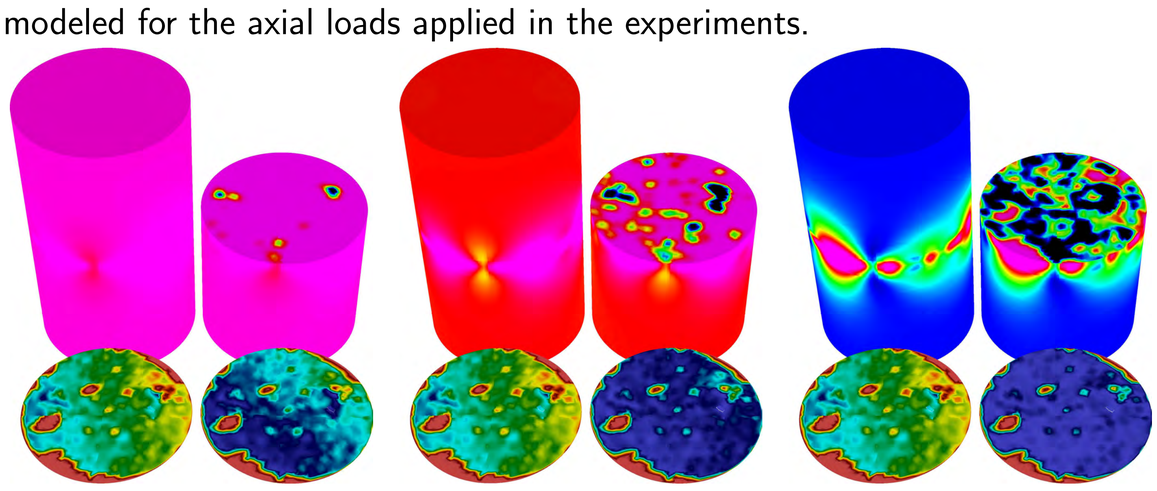

$\sigma_Z = 0.25$ *MPa* $\sigma_Z = 2$ *MPa* $\sigma_Z = 10$ *MPa*

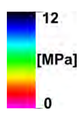

- top left: σ_Z
- top right: σ_Z (fracture)

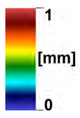

- bottom left: aperture a($\sigma_Z = 0$)
- bottom right: aperture a(σ_Z)

Fracture closure (experiments vs simulations)

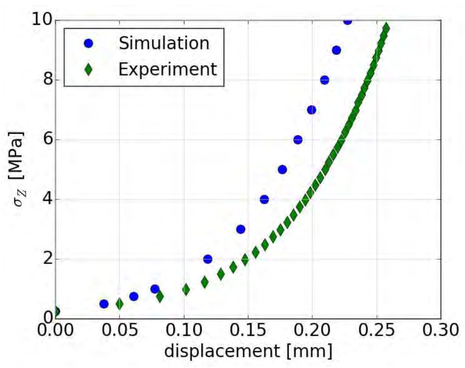

The model captures;

- Fracture contact stress evolution.
- Fracture closure and fluid pressure behavior captured with local cubic law.

Figure : Fracture closure vs σ_Z for experiment and simulation

References

1. Settgast, R. R., P. Fu, S. D. Walsh, J. A. White, C. Annavarapu, and F. J. Ryerson (2016), A fully coupled method for massively parallel simulation of hydraulically driven fractures in 3-dimensions, International Journal for Numerical and Analytical Methods in Geomechanics, submitted.
2. Vogler, D., R. R. Settgast, C. Annavarapu, P. Bayer, F. Amann (2016), Hydro-Mechanically Coupled Flow through Heterogeneous Fractures, in Stanford Geothermal Workshop, Stanford University Press, Palo Alto.
3. Vogler, D., F. Amann, P. Bayer, and D. Elsworth (2016), Permeability evolution in natural fractures subject to cyclic loading and gouge formation, Rock Mechanics and Rock Engineering, pp. 117, doi:10.1007/s00603-016-1022-0
4. Vogler, D., R. R. Settgast, C. Annavarapu, C. Madonna, P. Bayer, F. Amann, Experiments and Simulations of Fully Hydro-Mechanically coupled Response of Rough Fractures exposed to High Pressure Fluid Injection, in preparation

Reservoir scale application

- Domain size: 100m x 100m x 40m.
- Aperture field generation with aperture data obtained from rock cores.

1. Generate aperture field for zero-stress
2. Apply vertical load σ_Z.
3. Fluid injection in fracture center.
4. Fracture opening with increasing p_{inj}.

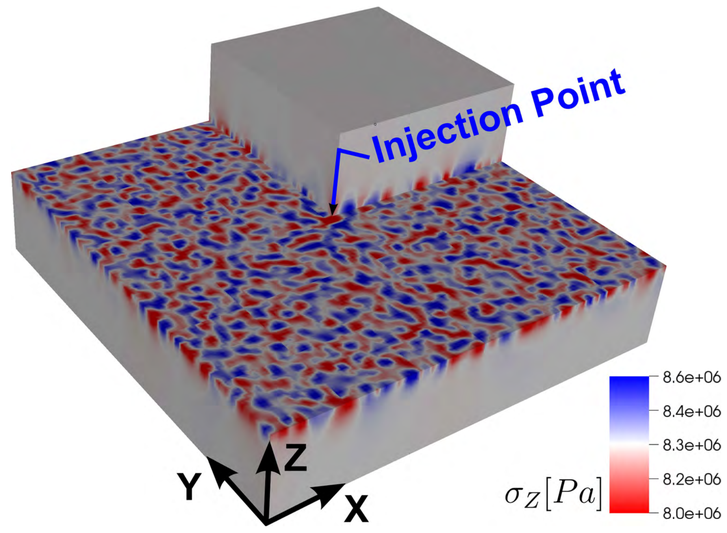

Figure : Vertical stress σ_Z distribution.

$\sigma_z = 0.0$ *MPa*

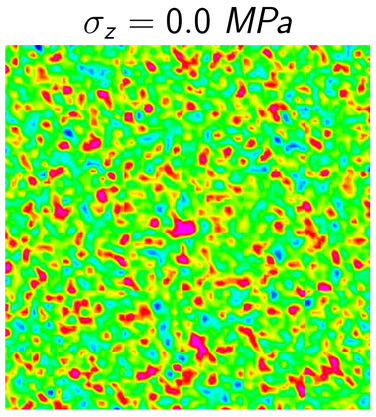

$\sigma_z = 8.3$ *MPa*

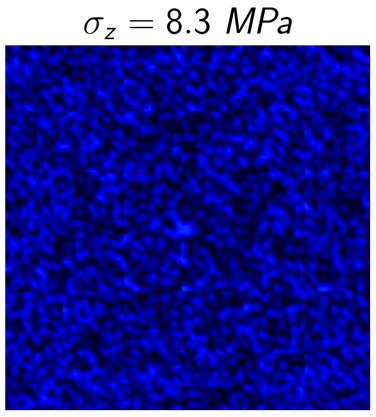

aperture a $[\mu m]$

Figure : Aperture distribution for varying σ_Z.

Simulating fluid injection in reservoir

Fluid injection into the fracture center results in localized fracture opening.

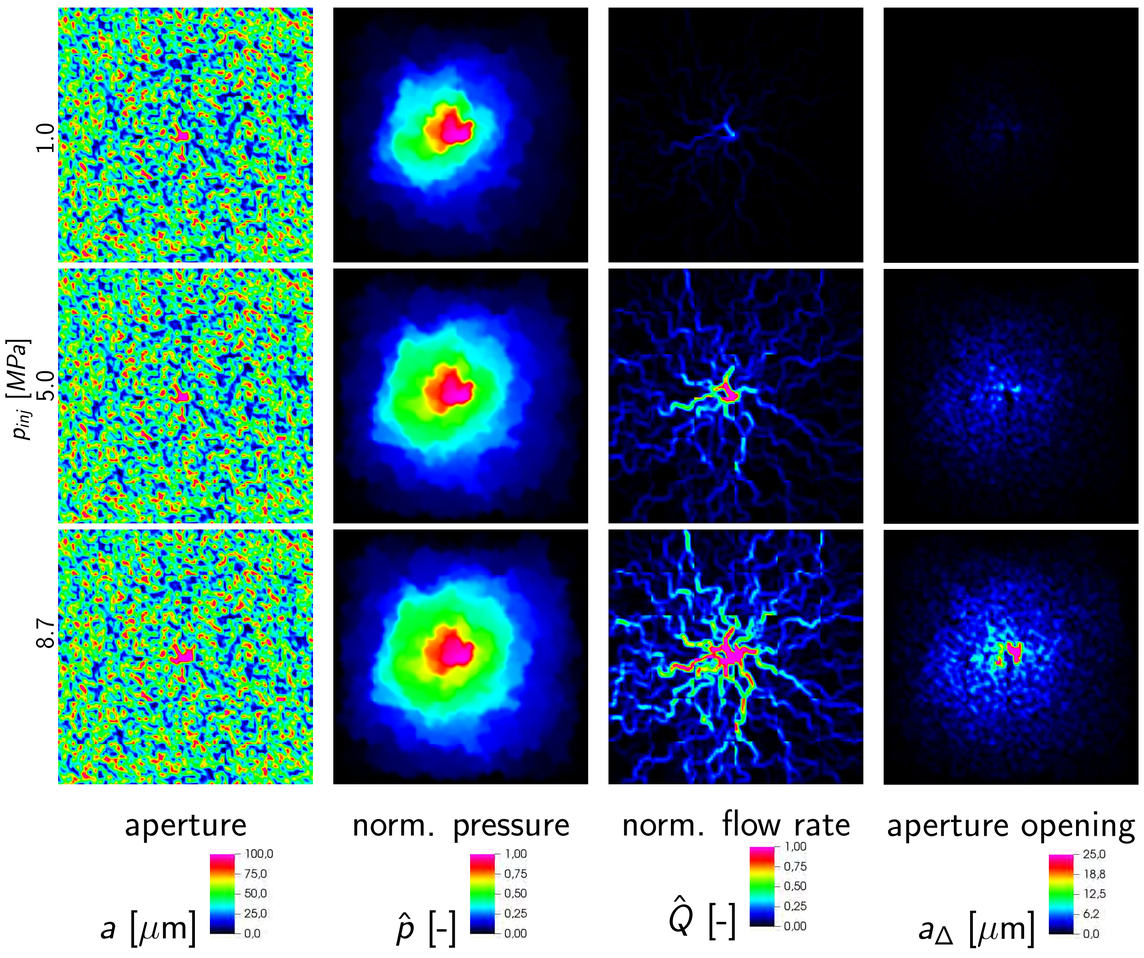

Injection flow rate vs injection pressure

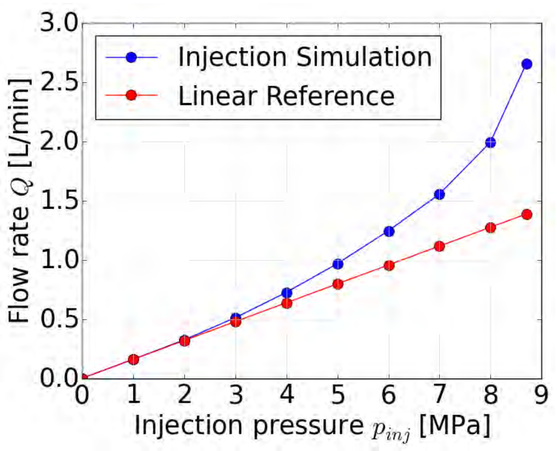

- Reservoir scale simulations load stage specific, unique aperture distribution.
- Fracture aperture opening during injection strongly localized.
- ⇒ Increasingly non-linear fracture opening and injection flow rate.

Figure : Flow rate response Q to increasing injection pressure p_{inj}.

Outlook

- Model shear dilation in heterogeneous fractures.
- Investigate scaling relations.
- Study impact of fracture connectivity on HM processes.

Contact: Daniel Vogler - davogler@erdw.ethz.ch

Fluid injection in a frictional weakening fracture

Nucleation and arrest of dynamic instability

Federico Ciardo[1] **& Brice Lecampion**[1]

EPFL - [1]Geo Energy Laboratory - Gaznat Chair on Geo-Energy (GEL)

federico.ciardo@epfl.ch, brice.lecampion@epfl.ch

ÉCOLE POLYTECHNIQUE FÉDÉRALE DE LAUSANNE

Schweizerische Eidgenossenschaft
Confédération suisse
Confederazione Svizzera
Confederaziun svizra

Swiss Federal Office of Energy SFOE

FNSNF
Fonds national suisse
Schweizerischer Nationalfonds
Fondo nazionale svizzero
Swiss National Science Foundation

Introduction

Understanding the mechanism of nucleation of dynamic rupture is an important issue in seismology since it is the key factor in determining the seismic potential of pre-existing faults under long-term loadings [2] [3] [4]. Furthermore, the activation of Mode II crack by means of fluid injection in a fracture is one of the mechanisms that enhance the permeability in deep geothermal reservoirs (Enhanced Geothermal Systems) whose efficacy rely on the shear-induced dilation.

Since we are interested in modelling a fracture network under hydraulic stimulation, a deep understanding of the shear crack propagation induced by fluid injection is needed.

Locally elevated pore pressure associated with fluid injection leads to a reduction of the fault frictional strength (product of the local normal effective stress and the slip-weakening friction coefficient) which may eventually falls below the background shear stress. As a result, a shear crack will start to propagate with an initially moderate velocity (quasi-static) as it is induced by fluid pressure diffusion. As slip accumulate, the quasi-static crack growth may become unstable due to the slip-weakening nature of friction, resulting in the nucleation of a dynamic rupture (micro-seismicity) until residual frictional strength is reached [1].

Theoretical and numerical models now exist to simulate shear fault/fracture under fluid injection for both quasi-static (QS) and quasi-dynamic (QD) crack growth. However, a comparison between the QS and QD approaches has not been done. Therefore the question that arises is how the inertial effects affect the dynamic instability and the rupture run-out distance.

Motivation

Being aware of the fact that instability due to frictional strength reduction may occur, the purpose of this study is to gain insight into the nucleation of dynamic rupture. The following questions will be researched: (I) Which are the parameters that govern the nucleation of dynamic instability? (II) Does the dynamic instability eventually arrest? (III) Which are the differences between the quasi-static (QS) and the quasi-dynamic (QD) approaches? (IV) What is the contribution in terms of instability of the viscous radiation damping term?

Quasi-static and quasi-dynamic shear crack propagation under fluid injection

Problem formulation

Let us consider a fracture of a given finite length $2a$ in the uniform background stress field characterised by the normal σ_n and shear τ^b components (Fig. 1a).

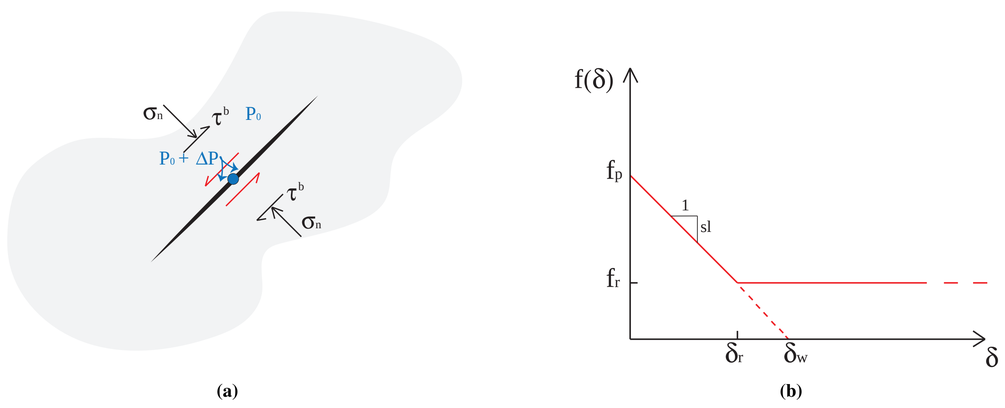

(a) (b)

Figure 1: a) Fracture geometry and loading conditions. b) Friction weakening law.

By solving the equation of continuum elastodynamics, it is possible to express the *quasi-dynamic formulation* of the stress history $\tau(x,t)$ on the fracture plane in terms of the slip history $\delta(x,t)$ [3] as

$$\tau(x,t) = \tau^b(x,t) - \frac{\mu^*}{2\pi}\int_{a_-(t)}^{a_+(t)} \frac{\partial\delta(s,t)}{\partial s}\frac{ds}{x-s} + \frac{\mu}{2c_s}\dot{\delta}(x,t) \tag{1}$$

where $\mu^* = \mu/(1-\nu)$, ν is the Poisson's ratio, μ is the shear modulus, c_s is the shear wave speed, $\dot{\delta}(x,t) = \partial\delta(x,t)/\partial t$ is the slip rate and $\tau^b(x,t)$ is the background stress (or loading stress). The term $\frac{\mu}{2c_s}$ is the viscous radiation damping term [4].

The *quasi-static formulation* of the elastic equilibrium is equal to Eq. 1 without the contribution of the inertial effects (damping term).

Within the fracture region, we consider the shear weakening Mohr-Coulomb criterion. Consequently, the shear stress must be lower (or equal) to the crack shear strength:

$$\tau \leq f(\delta)(\sigma_n - p), \tag{2}$$

where $\sigma_n - p$ (also denoted as σ') is the effective stress normal to the fracture and $f(\delta)$ is the friction weakening coefficient (see Figure 1b).

For the evolving pore pressure profile in the fracture, a profile with the following form is considered (which is the solution of pore pressure diffusion from a point source in the fracture with constant hydraulic diffusivity):

$$p(x,t) = p_0 + \Delta p \cdot Erfc\left(\left|\frac{x}{\sqrt{\alpha t}}\right|\right), \tag{3}$$

where α is the hydraulic conductivity and $Erfc$ is the $Complementary\ Error\ Function$.

Numerical scheme description

The coupling between the equation of QD (or QS) elastic equilibrium (Eq. 1) and the MC criterion (Eq. 2) is solved numerically using Displacement Discontinuity Method (with piecewise linear shear displacement discontinuities). The algorithm solves the coupled problem with an implicit scheme: in one increment of time it solves implicitly Eq. 1 and at the same time it enforces the MC criterion (Eq. 2). The scheme is similar to a radial return algorithm for plasticity: the violation of the Mohr-Coulomb criterion (due to the fluid diffusion in the fracture) leads to an excess of shear stress that has to be released (through the slip). Consequently the shear stress history is updated according to the Q-D or Q-S formulation until the M-C criterion is satisfied everywhere along the fracture.

Results

Solutions of the governing equations (in terms of normalized crack half-length a/a_w and normalized peak slip δ/δ_w) as a function of normalized time $\sqrt{\alpha t}/a_w$, understress $(\tau_p - \tau^b)/\tau_p$, overpressure $\Delta p/\sigma'_0$ and $f_r/f_p = 0.6$ are hereunder reported (for the scaling: $a_w = \frac{\mu^*\delta_w}{\tau_p}$ and $\delta_w = \frac{f_p}{sl}$).

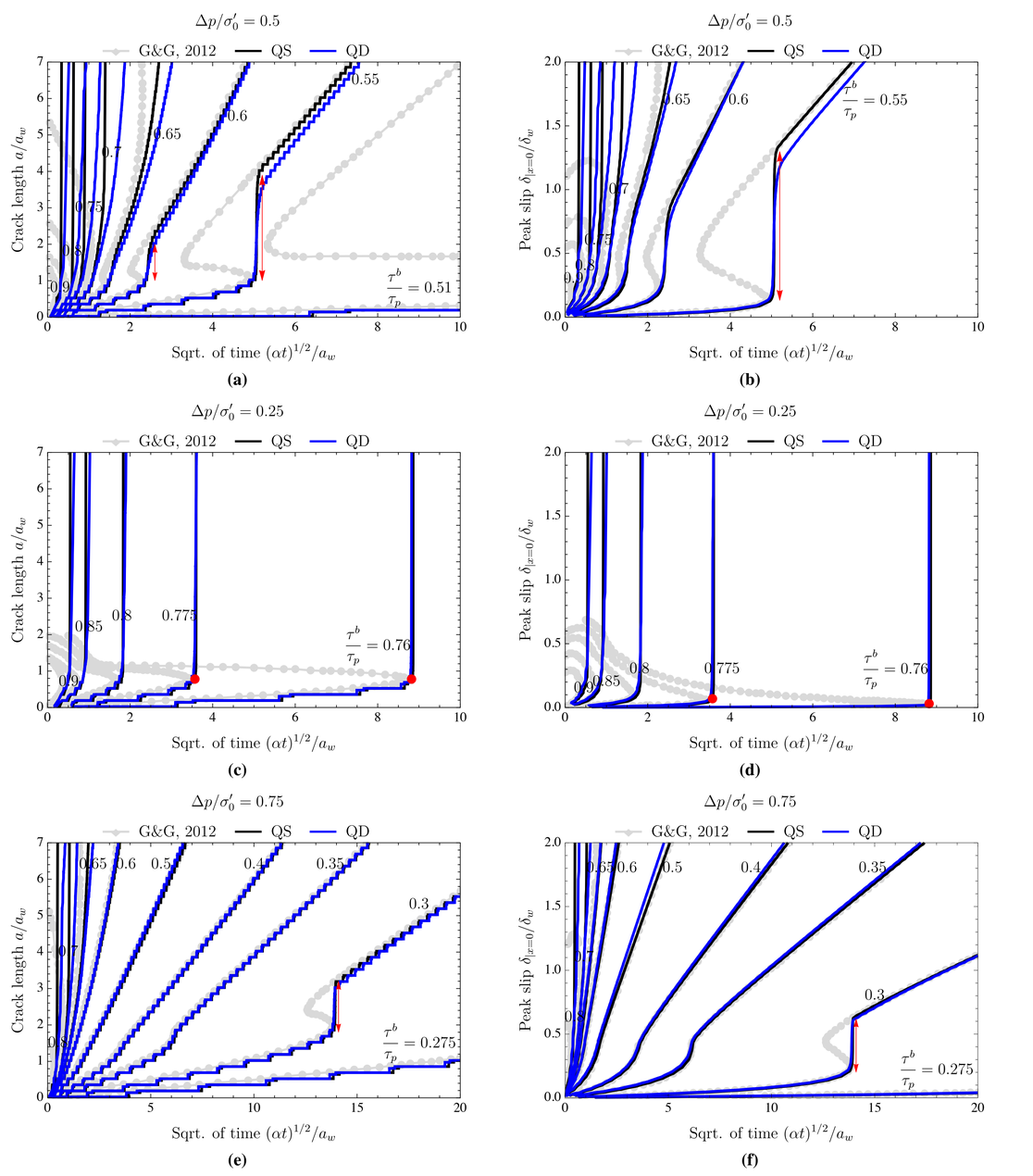

(a) (b) (c) (d) (e) (f)

Figure 2: QS and QD development of the normalized crack half-length (a-c-e) and the slip at the crack center (b-d-f) for various values of the normalized fracture background stress τ^b/τ_p and three values of constant overpressure. The marked line corresponds to the G&G's results (2012) of quasi-static crack propagation (benchmark).

Conclusions

- Figure 2 shows that our code matches perfectly the semi-analytical solution of G&G (2012).
- The quasi-static expansion of slipping zone (paced by pore pressure diffusion) may eventually leads to instability and transition into dynamic rupture.
- Furthermore, depending on the loading conditions, initial shear stress state and residual friction coefficient, the dynamic instability can be potentially arrested.
- Although counterintuitive, the dynamic run-out distance is the largest for the lowest value of fluid overpressure, because the higher is the overpressure the quicker the residual frictional strength of the fracture is reached.
- The viscous radiation damping term leads to a slightly lower stress drop and slip. Consequently the length of the nucleation path is reduced and the transition between the dynamic instability and the quasi-static crack growth is smoother.

Forthcoming Research

The new step will be to include in the model the shear dilatancy of the fracture (by coupling the deformation with the fluid flow in the fracture). Dilatancy tends to increase the local normal *effective* stress and thus will inhibit the dynamic instability.

References

[1] Garagash, D.I., Germanovich, L.N., 2012. Nucleation and arrest of dynamic slip on a pressurized fault. *J. Geophys. Res.*, 117, B10310, doi:10.1029/2012JB009209.

[2] Lapusta, N., Liu, Y., 2009. Three-dimensional boundary integral modeling of spontaneous earthquake sequences and aseismic slip. *J. Geophys. Res.*, 114, B09303.

[3] Lapusta, N., Rice, J.R., 2000. Elastodynamic analysis for slow tectonic loading with spontaneous rupture episodes on faults with rate- and state-dependent friction. *J. Geophys. Res.*, 105(B10), p.23,765-23,789.

[4] Rice, J.R., 1993. Spatio-temporal Complexity of Slip on a Fault. *J. Geophys. Res.*, 98(B6), p.9885-9907.

The tip region of a hydraulic fracture driven by a power law fluid

Fatima-Ezzahra Moukhtari*, Brice Lecampion*

* Geo-Energy Laboratory - Gaznat Chair on Geo-Energy (GEL), Ecole Polytechnique Federale de Lausanne (EPFL)

fatima-ezzahra.moukhtari@epfl.ch, brice.lecampion@epfl.ch

FONDS NATIONAL SUISSE
SCHWEIZERISCHER NATIONALFONDS
FONDO NAZIONALE SVIZZERO
SWISS NATIONAL SCIENCE FOUNDATION

1. Introduction

The problem of a fluid-driven fracture propagating in an elastic isotropic medium is a subject of great importance in the hydraulic fracturing process and also in the oil and gas industry. We present here numerical tip region solutions for fracture width and pressure when a Non-newtonian fluid drives a semi-infinite fracture in an impermeable linear solid. We account for the presence of lag of a priori unknown length between the fluid front and the crack tip. The fluid studied is a power law shear thinning fluid flowing in the fracture under the hypothesis of lubrication flow. For such a rheology, in simple shear, the fluid shear stress τ is linked to the shear rate $\dot{\gamma}$ as follows:

$$\tau = M\dot{\gamma}^n$$

where n is the fluid index ($n < 1$ for shear-thinning fluid) and M is the consistency index.

2. Problem statement

Consider the propagation of a semi-infinite two-dimensional fracture with a constant velocity V in an impermeable elastic isotropic medium characterised by plane strain elastic modulus E' and fracture toughness $K' = \sqrt{\frac{32}{\pi}} K_{Ic}$. The fracture is loaded internally by the fluid (whose pressure p_f is part of the problem solution) and by the far-field confining stress σ_o. The fracture is assumed to propagate (along x-axis) in mobile equilibrium ($K_I = K_{Ic}$).
Our numerical results include the fracture opening $w(x)$ and the net pressure $p(x) = p_f(x) - \sigma_o$ profiles over the whole fracture as well as the corresponding value of the fluid lag size.
The solid deformation is given by the equations of linear elastic fracture mechanics which links the net pressure to the fracture opening [2]

$$p(x) = \frac{E'}{4\pi} \int_0^\infty \frac{\partial w}{\partial x} \frac{\partial s}{x - s}$$

The fluid flow inside the fracture is described by the width average solution for lubrication flow in a channel, for $x \in]\lambda, \infty[$

$$q|q|^{n-1} = \frac{w^{2n+1}}{M'} \frac{\partial p}{\partial x}$$

where $M' = \frac{2^{n+1}(2n+1)^n}{n^n} M$.
In the moving system, the flow rate q per unit width is simply reduced to $q = Vw$. In the lag region, the fluid pressure is neglected: $p = -\sigma_o$ for $x \in [0, \lambda]$.
The quasi-static fracture propagation $K_I = K_{Ic}$ is equivalent to prescribing the width asymptote as: $w = \frac{K'}{E'} x^{1/2}$, $x \to 0$

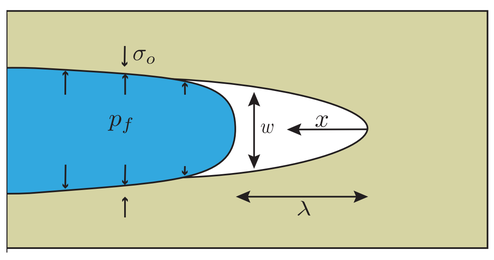

Figure 1: *Sketch of semi-infinite fluid-driven fracture propagating at constant velocity V in an impermeable medium.*

3. Results

We introduce the dimensionless variables of the problem using two lengthscales L_μ and L_κ

$$\Omega = \frac{E'w}{\sigma_o L_\mu}, \qquad \Pi = \frac{p - \sigma_o}{\sigma_o}, \qquad \xi = \frac{x}{L_\mu}$$

where

$$L_\mu = V \left(\frac{M'}{\sigma_o}\right)^{1/n} \left(\frac{E'}{\sigma_o}\right)^{\frac{n+1}{n}}, \qquad L_k = \left(\frac{K'}{\sigma_o}\right)^2$$

The solution of the problem actually only depends on the value of the fluid power law index n and a dimensionless toughness κ function of all the problem parameters:

$$\kappa = \left(\frac{1}{V}\right)^{1/2} \left(\frac{\sigma_o^{2-n}}{M' E'^{n+1}}\right)^{1/2n} K'$$

The nonlinear system of equations is discretised using Gauss-Chebyshev polynomials [3]. This technique uses trigonometric values for the abscissas and the collocation points as made when using the Gauss-Chebyshev for solving singular integral equations corresponding to finite cracks. Therefore, we transform the coordinate from the semi-infinite interval $[0, \infty[$ to the finite interval $[-1, 1[$. The resulting non-linear system of equations is solved via a quasi-Newton root-finding scheme using the dimensionless net pressure at the collocation points as the primary unknown variables.

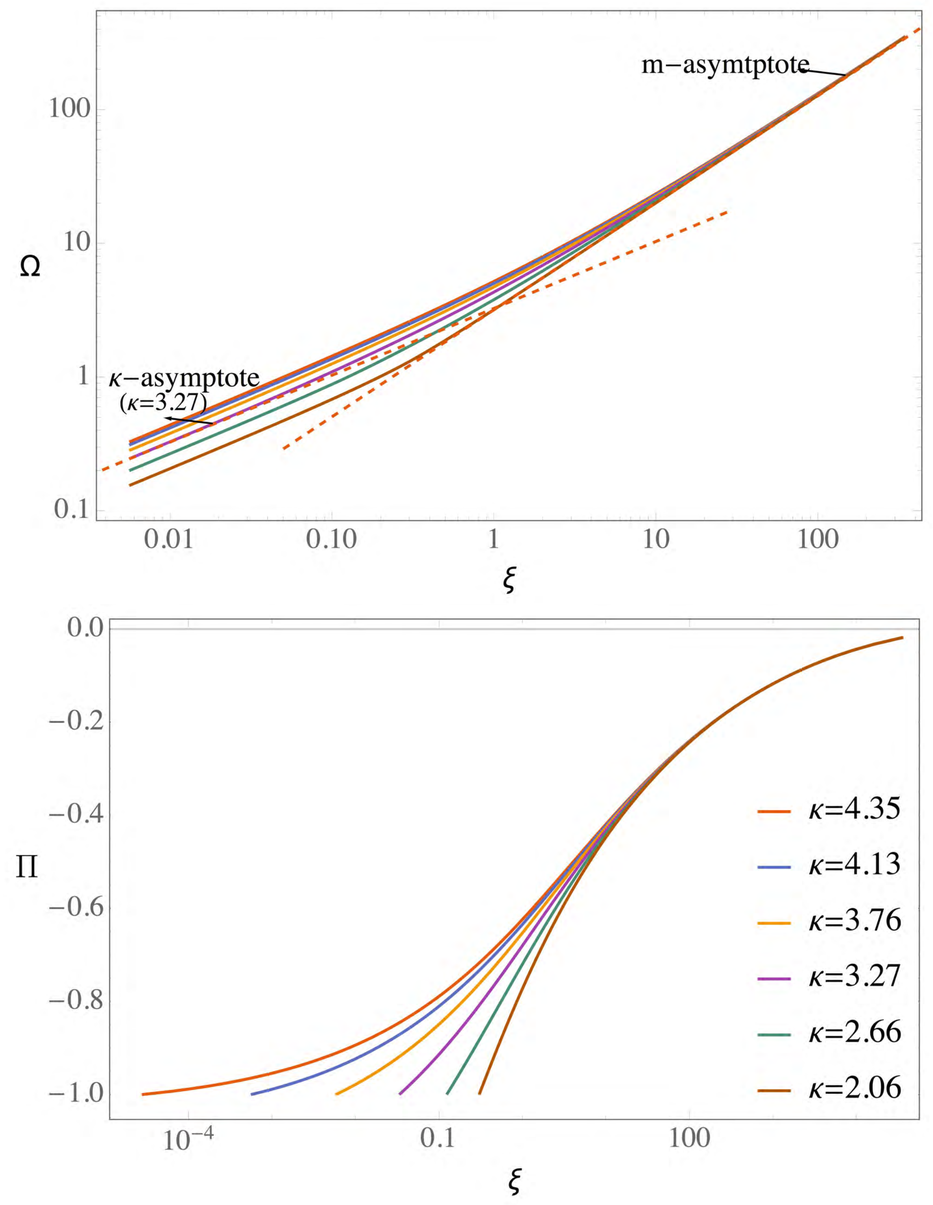

Figure 2: *Example of dimensionless opening Ω (in log-log scale) and net pressure Π (in semi-log scale) respectively along the fracture for different toughness ($n = 0.5$).*

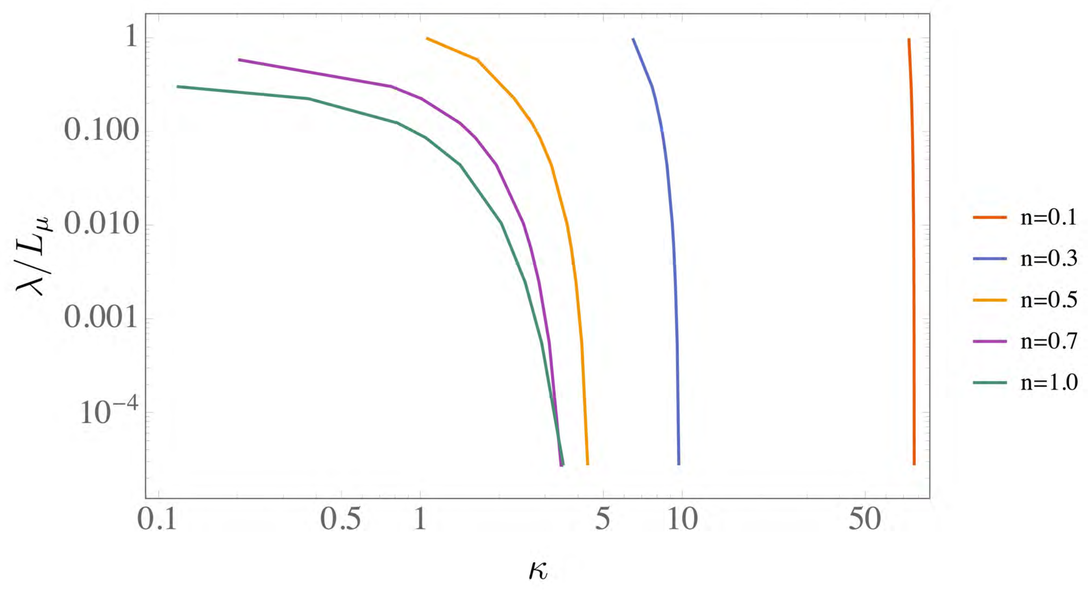

Figure 3: *Dimensionless fluid lag λ/L_μ (in log-log scale) with respect to the dimensionless toughness κ for the different fluid index n.*

***κ*-asymptote**: $\Omega = \kappa\sqrt{\xi}$
***m*-asymptote**: $\Omega = (\frac{2(n+2)^2}{n} \tan(\frac{-2\pi}{n+2}) \xi^2)^{\frac{1}{n+2}}$

We show that the solution is not only consistent with the square root singularity of linear elastic fracture mechanics near the tip ($x \ll L_\mu$) (κ-asymptote), but that its asymptotic behaviour in the far field ($x \gg L_\mu$) corresponds to the solution of a semi-infinite hydraulic fracture driven by a power-law fluid constructed on the assumptions of zero toughness and zero fluid lag (so-called m-asymptote [1]). Our results also document how the power-law index modify the variation of the lag size as a function of the dimensionless toughness κ, and its disappearance for large value of κ.

References

[1] DESROCHES, J., DETOURNAY, E., LENOACH, B., PAPANASTASIOU, P., PEARSON, J., THIERCELIN, M., AND CHENG, A. The crack tip region in hydraulic fracturing. In *Proceedings of the Royal Society of London A: Mathematical, Physical and Engineering Sciences* (1994), vol. 447, The Royal Society, pp. 39–48.

[2] GARAGASH, D., AND DETOURNAY, E. The tip region of a fluid-driven fracture in an elastic medium. *Journal of applied mechanics 67*, 1 (2000), 183–192.

[3] IOAKIMIDIS, N., AND THEOCARIS, P. The practical evaluation of stress intensity factors at semi-infinite crack tips. *Engineering Fracture Mechanics 13*, 1 (1980), 31–42.

SCCER SoE
SWISS COMPETENCE CENTER for ENERGY RESEARCH
SUPPLY of ELECTRICITY

SCCER-SoE Annual Conference 2016

In cooperation with the CTI
Energy
Swiss Competence Centers for Energy Research
Schweizerische Eidgenossenschaft
Confédération suisse
Confederazione Svizzera
Confederaziun svizra
Swiss Confederation
Commission for Technology and Innovation CTI

Finite element modeling of three-dimensional fracture growth using unstructured tetrahedral meshes

Morteza Nejati, Thomas Driesner
SCCER-SoE, ETH Zurich, Switzerland

Introduction

Understanding the hydraulic fracturing processes in enhanced geothermal reservoirs (EGS) requires sophisticated numerical methodologies for modelling fracture growth accurately. Three-dimensional fracture growth modelling under complex *in-situ* stress and fluid-driven loadings is a difficult task due to complicated geometry of fractures which often occur by turning and twisting of hydraulic fractures. The numerical implementation of the fracture growth also requires that these complex non-planar geometries to be updated in every increment, building a new geometry for the simulator in the next increment. On the other hand, standard finite element approaches for crack growth simulation rely on the update of mesh which has to conform to the fracture surfaces. Robust and automatic remeshing of fractured bodies are feasible only with unstructured tetrahedral meshes because structured meshes based on other types of elements are extremely difficult to be employed in complex geometries. Therefore, reliable methods for simulating fracture growth based on unstructured meshes have to developed.

Methodology

The development of algorithms for growing cracks using standard finite element approaches involves three steps: (i) Solving the boundary value problem for the current loading conditions, and computing the fracture parameters such as the stress intensity factor and the J-integral for all cracks in the domain. (ii) Employing a well-validated crack propagation criterion to estimate the angle and the extent of the crack growth of segments over the crack front. (iii) Change the geometry by extending the crack and continue the simulation from step i. In this algorithm the crack growth process is subdivided into several increments where the cracks advance until the energy released due to crack growth is not large enough to overcome the surface energy required to advance the crack. During all the increments, the boundary value problem is solved to satisfy the equilibrium condition throughout the model. For a fixed set of boundary conditions, the model is iteratively deformed, until no more growth is registered. Since the mesh is dependent on the geometry of the crack, after crack advance in each increment the domain has to be remeshed in order to capture the emerging crack geometry. In every increment the geometry changes, the previous stress state is invalidated and new updated stresses are re-computed. In summary, the simulation of fracture growth involves the following steps [1,2]:

1- Generate the geometry and mesh automatically
2- Apply boundary conditions and Solve for deformation
3- Compute fracture parameters
4- Compute propagation angle and length, and extend cracks
5- Remesh the new geometry and map the variables
6- Go to step 2 unless no growth is registered for this increment

Results

In order to demonstrate the efficiency and accuracy of the crack growth simulation using unstructured tetrahedral elements, two cases of fracture growth under uniaxial tension are shown in Figs. 1 and 2. Fig. 1 shows the incremental growth of a single penny-shaped crack oriented at the angle 45° with respect to the direction of load. Fig. 2 also shows this incremental growth but for a highly fractured medium, where fifty randomly-oriented cracks are growing simultaneously. In such a model, the interaction of nearby cracks can considerably influence the growth path. The results of the simulation of crack growth show that a growth simulator based on tetrahedral elements is efficient and accurate to predict paths of single and multiple interacting cracks. All crack growth procedures including incremental geometry change, remeshing, and mapping have been implemented into the CSMP++ based Geomechanics Toolkit of Imperial College London [1, 2].

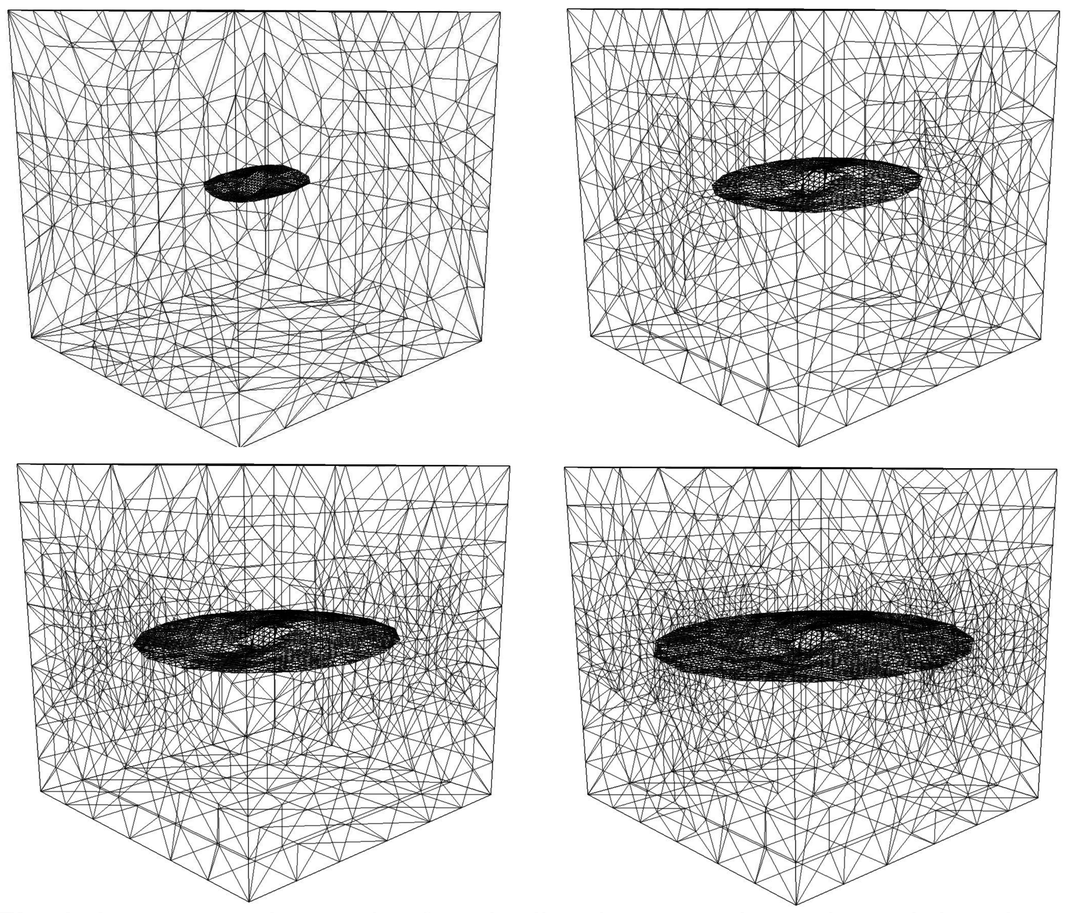

Fig 1. Incremental growth of an inclined penny-shaped crack in a large cube subjected to uniaxial tension [2].

Fig 2. Incremental growth of fifty interacting randomly-oriented penny-shaped cracks in a large cube subjected to uniaxial tension [2].

Conclusions

Since tetrahedral meshes are suitable for meshing complex geometries with multiple cracks, a growth simulator based on tetrahedral elements can be efficiently used to investigate the complex coupled fracturing processes in enhanced geothermal systems where multiple interacting fractures may be developed and coalesce. Potential incorporation of hydraulic and thermal effects in this numerical methodology is also straightforward.

References

(1) Paluszny, A. and Zimmerman, R. W. (2011). Numerical simulation of multiple 3D fracture propagation using arbitrary meshes. Computer Methods in Applied Mechanics and Engineering, 200:953–966.
(2) Nejati, M., 2015. Finite element modelling of frictional contact and stress intensity factors in three-dimensional fractured media using unstructured tetrahedral meshes. PhD thesis, Imperial College, London, UK.

SCCER SoE

SWISS COMPETENCE CENTER for ENERGY RESEARCH
SUPPLY of ELECTRICITY

SCCER-SoE Annual Conference 2016

In cooperation with the CTI

Energy
Swiss Competence Centers for Energy Research

Schweizerische Eidgenossenschaft
Confédération suisse
Confederazione Svizzera
Confederaziun svizra

Swiss Confederation

Commission for Technology and Innovation CTI

Characterization of the in-situ stress field at Grimsel Test Site

H. Krietsch, N. Dutler, V. Gischig, B. Valley, K. Evans & F. Amann

Motivation

In the first phase of the In-situ Stimulation and Circulation (ISC) experiment at Grimsel Test Site (GTS) a detailed stress characterization campaign was conducted. It consisted of in-situ stress measurements (i.e. overcoring and hydraulic fracturing) and a numerical modelling study to validate the measured far-field stress tensor. The exact knowledge of the stress situation is of crucial importance for the stimulation experiment and the possibility for fracture slip movement.

Methods: In-situ stress measurements

The in-situ stress measurement campaign combined stress relief methods (overcoring of 10 USBM and 6 CSIRO-HI probes) and 10 hydraulic fracturing tests in three boreholes. Subsequent biaxial tests of overcored specimens were conducted to measure the elastic moduli. The fracture propagation orientation during HF was recorded with a micro-seismic monitoring system and the trace of the induced fracture at the wellbore wall was visualized using an imprint packer.

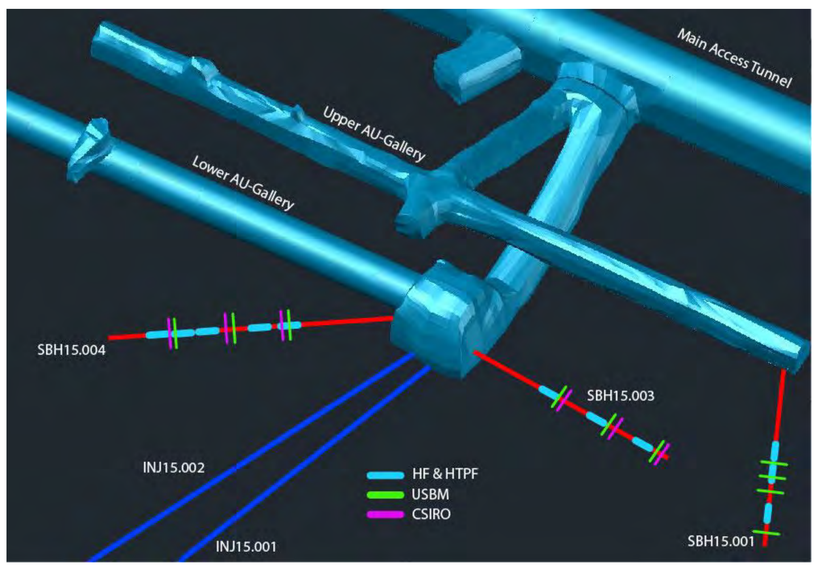

Figure 1: Locations of stress measurements

Methods: Numerical Modelling

The modelling work is performed with the 3D distinct element code 3DEC from ITASCA. The model starts with a cuboid measuring 5600 x 5600 x 3500 m and smaller prisms approximating the topography. The GTS is imbedded in the center of the cuboid at 1734 m amsl. Roller boundary conditions are applied. Shortening in directions striking 105-285° (MOD105) and 150-330° (MOD150) is needed to reproduce both the orientation and magnitude of the stress tensor derived from HF and overcoring, respectively. The constitutive model is described by a bi-linear failure envelope (Leith et al., 2014).

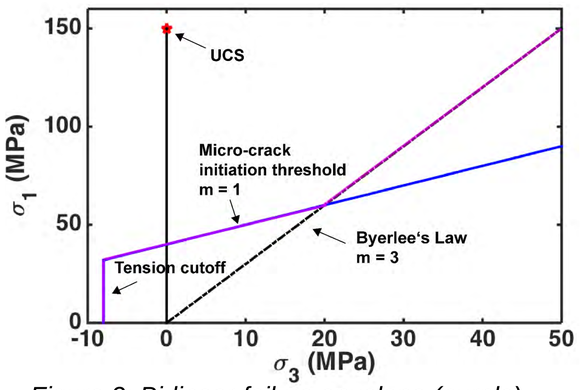

Figure 2: Bi-linear failure envelope (purple).

Using the resulting stress tensor, a slip-tendency analysis is performed.

Results

In-situ overcoring measurements indicate σ_1 is sub-horizontal, and dips towards SE. σ_2 and σ_3 are relatively steeply inclined and dip towards NE and SW, respectively. The principal stress magnitudes are 18 MPa, 12 MPa and 9 MPa. Microseismic monitoring during HF indicated a nearly EW striking σ_1 and a sub-horizontal σ_3 that points towards SWS.

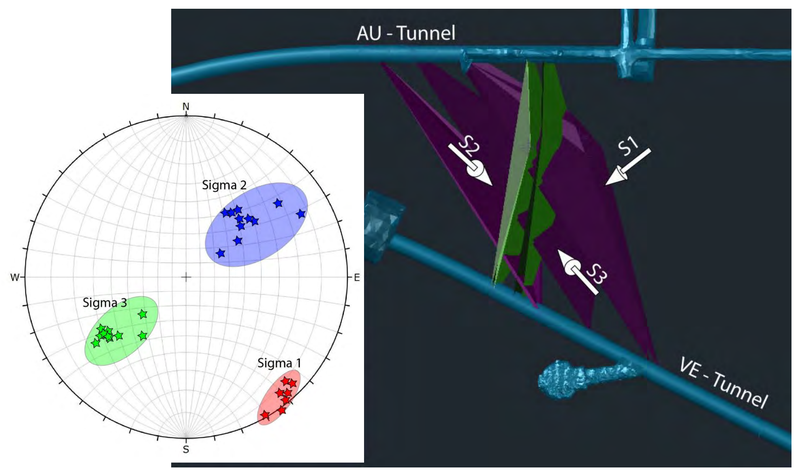

Figure 3: Principal stresses in respect to major shear zones and stereoplot (lower hemisphere)

The numerical stress models that assume a regional loading direction striking 150-330° (MOD150) fit best with the overcoring measurements.

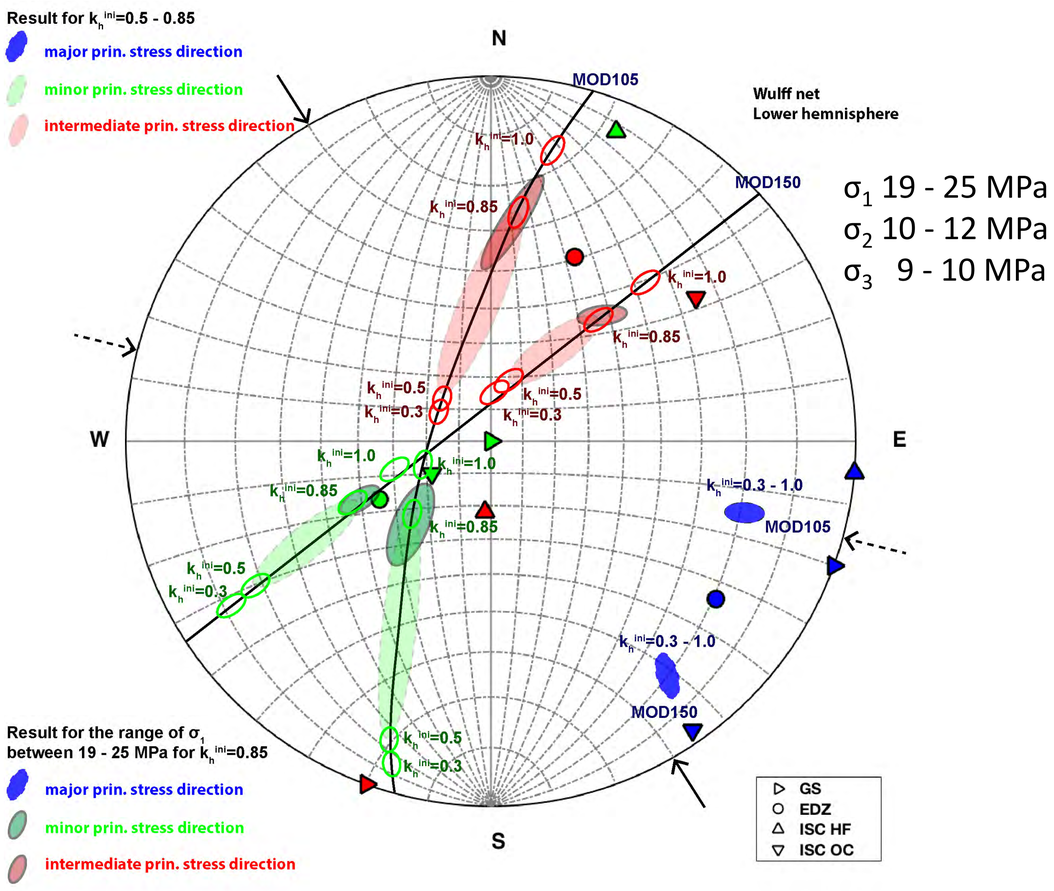

Figure 4: Results from MOD150 and MOD105 for four different minimal horizontal initial stress states k_h^{ini} and a maximal horizontal initial stress state k_H^{ini}=1 is indicated by the small ellipses.

The consistency between high-confidence overcoring results and numerical modelling suggest that the stress tensor given in Figure 3 is the most likely scenario, although there is some evidence of stress heterogeneity within the test volume. The slip-tendency analysis indicates that slip along geological structures, in particular S3, is likely during stimulation.

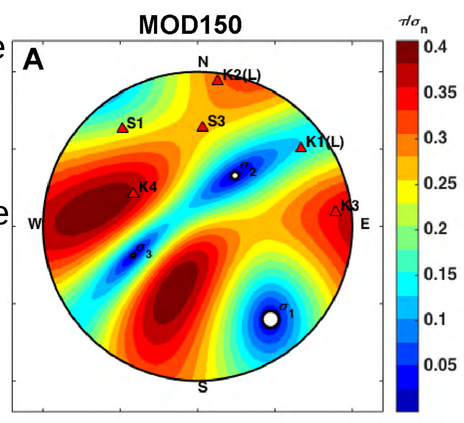

Figure 5: Slip tendency analysis

References

Amadei, B., & Stephansson, O. (1997). Rock Stress and Its Measurements. Springer International Publishing AG. doi: 978-94-011-5346-1

Konietzky, H., & Marshall, P. (1996). Excavation disturbed zone around tunnels in fractured rock – Example from the Grimsel Test Site. In Z. Rakowski (Ed.), Geomechanics (p. 235 - 240). Rotterdam/ Brookfield: A.A. Balkema.

Leith, K., Moore, J. R., Amann, F., & Loew, S. (2014). In situ stress control on microcrack generation and macroscopic extensional fracture in exhuming bedrock. J. Geophys. Res. Solid Earth, 119, 594-615.

Pahl, A., Heusermann, S., Bräuer, V., & Glöggler,W. (1989). Rock Stress Investigations (Tech. Rep. No. NTB88-39E). Wettingen: Nagra.

Conclusion

- High-quality overcoring tests yield results that are broadly in accord with the modeling analysis.
- There are inconsistencies between the overcoring results and the hydrofrac tests that provide evidence for stress heterogeneity within the test volume.
- The pattern of microseismicity during the hydrofracture tests is not consistent with simple mode-1 fracture propagation normal to the overcoring-derived σ_3 direction.
- Slip-tendency analysis shows that geological structures are favourably oriented for fracture slip during stimulation within the given tectonic stress field

SCCER SoE
SWISS COMPETENCE CENTER for ENERGY RESEARCH
SUPPLY of ELECTRICITY

SCCER-SoE Annual Conference 2016

In cooperation with the CTI
Energy
Swiss Competence Centers for Energy Research
Schweizerische Eidgenossenschaft
Confédération suisse
Confederazione Svizzera
Confederaziun svizra
Swiss Confederation
Commission for Technology and Innovation CTI

A slip induced stress transfer model for embedded discrete fractures

Gunnar Jansen, Stephen A. Miller
Centre for Hydrogeology and Geothermics - University of Neuchâtel

Motivation

A large fraction of the world's water and energy resources are located in naturally fractured reservoirs within the earth's crust. Understanding the dynamics of such reservoirs in terms of flow and transport is crucial to successful application of engineered geothermal systems (also known as enhanced geothermal systems or EGS) for geothermal energy production in the future. Heterogeneous in-situ stress dominates the reservoir development characteristics such as permeability creation and induced seismicity. Additionally, reservoir stimulation itself changes the local stress field due to thermo- and poro-elastic effects as well as slip induced stress transfer. Thus modeling the stress changes is of major importance in order to understand and predict reservoir development and mitigate the risk of induced seismicity.

Stress transfer in porous media

Various effects contribute to stress transfer in porous media. The major contributions relevant for geothermal systems are the fluid pressure, temperature differences and fracture slip.

- *Poroelastic contribution*
- Due to the fluid pressure, the local stress field is disturbed. Mathematicall this is described by the Biot equation [1] which can be simplified to Terzaghi's effective stress principle: $\sigma_{eff} = \sigma - p_f$
- $$\Rightarrow \Delta\sigma_{p_f} = -p_f$$
- *Thermoelastic contribution*
- Thermal expansion is the driving mechanism for thermally induced stress changes. A first order approximation yields a linear temperature dependence:
- $$\Rightarrow \Delta\sigma_T = D \cdot \alpha \cdot \Delta T$$
- *Slip induced stress change*
- We account for slip-induced stress changes based on Okada's analytical formulas derived from a Green's function solution to the elastic half space problem [2]. The stress change is heavily dependent on the type of motion (cf. Figure 1)

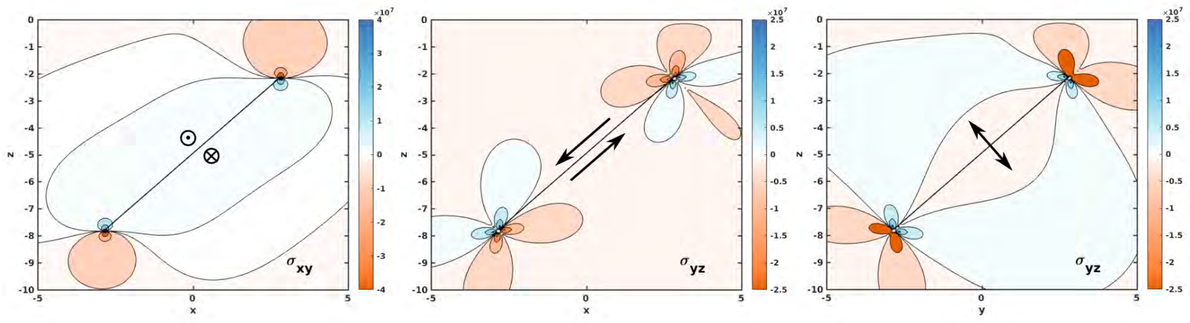

Figure 1: Shear stress induced by different types of fracture motion. *Left:* Strike-slip (out of plane) *Middle:* Dip-slip (also known as normal/reverse slip) / *Right:* Tensile motion

The total Stress change in the porous medium is obtained by superposition of the constituents:

$$\Rightarrow \Delta\sigma = \Delta\sigma_{p_f} + \Delta\sigma_T + \Delta\sigma_u$$

Numerical Method: Embedded discrete fracture model

The conceptual idea of the EDFM is the separation of a fractured reservoir into a fracture and a damaged matrix domain. A transfer function accounts for coupling effects between the two domains (Figure 2). Fracture and matrix domains are computationally independent except for the transfer function. As the fractures are generally very thin and highly permeable compared to the surrounding matrix rock this allows for a lower dimensional representation of fractures.

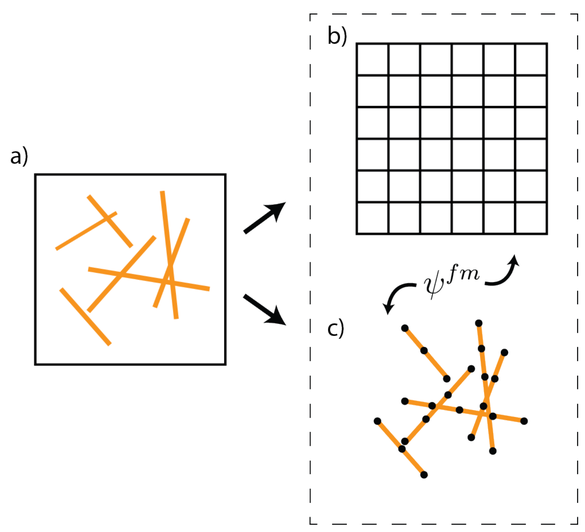

Figure 2: A fractured domain a) is separated in a uniform grid b) and a fracture grid c). The two resulting domains are coupled using the transfer function ψ_{fm} .

Results

The effects of stress transfer during seven days of fluid injection into a fractured reservoir are investigated. Simulation results for 100x100 matrix grid cells and 1153 fracture segments.

Table 1: Properties used in the fluid injection simulation. Subscripts: *fr* - fracture, *m* - matrix, *f* - fluid , *r* - rock.

Permeability	$K_{fr} = 10^{-12}$ m²	$K_m = 10^{-16}$ m²
Porosity	$\Phi_{fr} = 0.3$	$\Phi_m = 0.1$
Viscosity	$\nu = 10^{-4}$ kg/m/s	
Density	$\rho_f = 1000$ kg/m3	$\rho_r = 1000$ kg/m3
Specific heat	$c_{p,f} = 4000$ J/(kg*K)	$c_{p,r} = 900$ J/(kg*K)
Heat conductivity	$\Lambda_f = 0.5$ W/(m*K)	$\Lambda_r = 2.0$ W/(m*K)
Thermal expansion coeff.	$\alpha = 7.9 * 10^{-6}$ K^{-1}	
Shear modulus	G = 29.0 GP a	
Poisson ratio	$\nu = 0.25$	

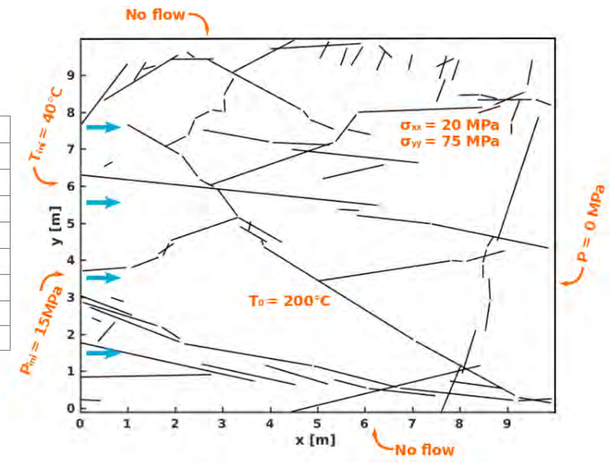

Figure 3: The model setup. The fracture network is based on the mapped fractures in a granite block [3].

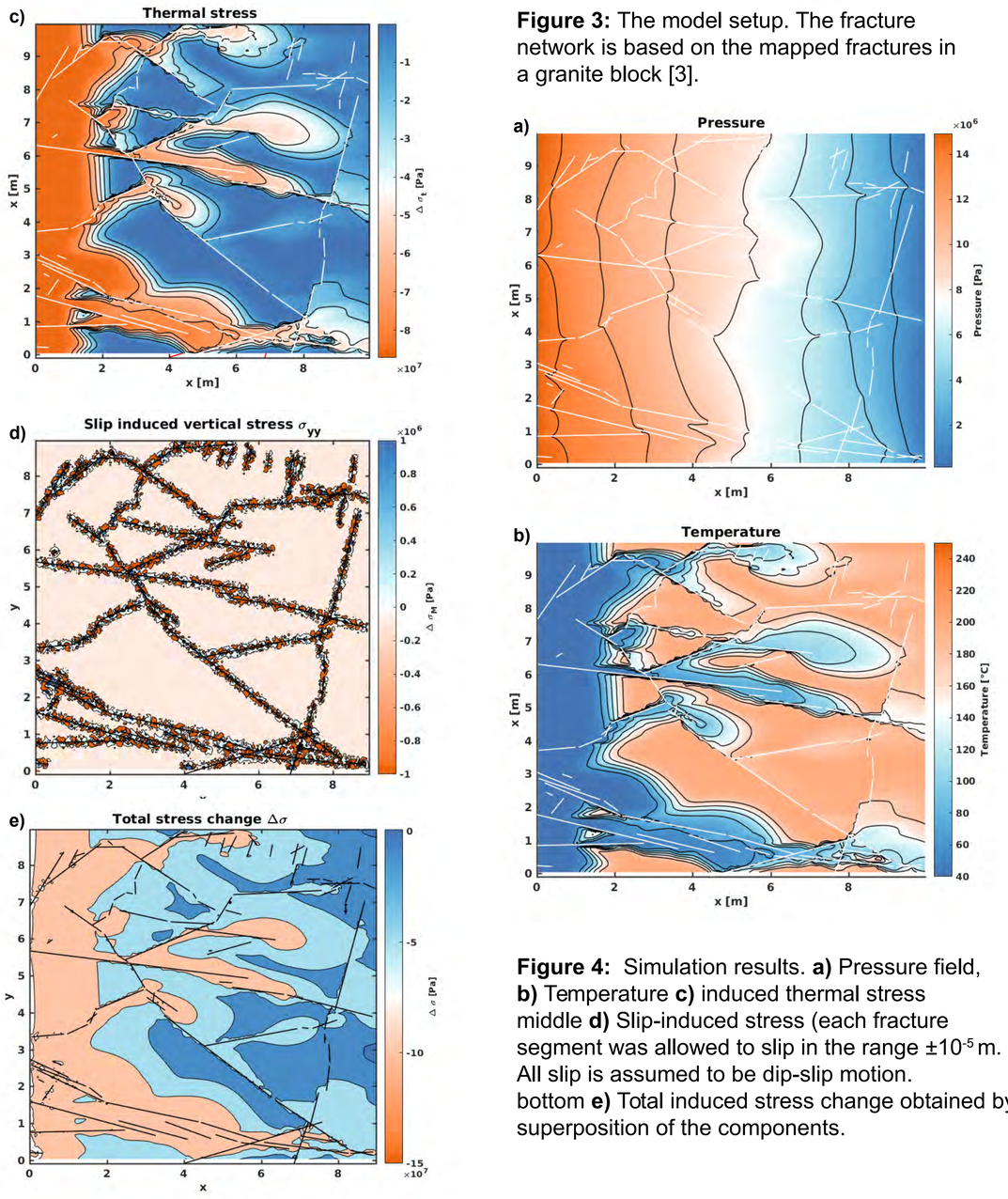

Figure 4: Simulation results. **a)** Pressure field, **b)** Temperature **c)** induced thermal stress middle **d)** Slip-induced stress (each fracture segment was allowed to slip in the range $\pm 10^{-5}$ m. All slip is assumed to be dip-slip motion. bottom **e)** Total induced stress change obtained by superposition of the components.

Conclusion

Using the presented stress transfer model the stress changes induced during the injection period of reservoir development can efficiently be studied. Future work will focus on coupling the results from the stress transfer model back to the flow and transport code which has been neglected here (cf. Figure 5).

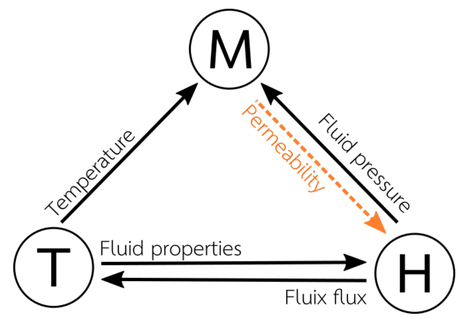

Figure 5: The current model's transfer functions (black) and the future model's added permeability transfer to allow dynamic fracture network evolution.

References

[1] Biot, M. A. (1941). General theory of three-dimensional consolidation. *Journal of applied physics*, 12(2), 155-164.
[2] Okada, Y. (1992). Internal deformation due to shear and tensile faults in a half-space. *Bulletin of the Seismological Society of America*, 82(2), 1018-1040.
[3] Dowd, P. A., et al. (2009). A three-dimensional fracture network data set for a block of granite. *International Journal of Rock Mechanics and Mining Sciences,* 46(5), 811-818.

SCCER SoE

SWISS COMPETENCE CENTER for ENERGY RESEARCH
SUPPLY of ELECTRICITY

SCCER-SoE Annual Conference 2016

In cooperation with the CTI

Energy
Swiss Competence Centers for Energy Research

Schweizerische Eidgenossenschaft
Confédération suisse
Confederazione Svizzera
Confederaziun svizra

Swiss Confederation

Commission for Technology and Innovation CTI

Physical Rock Properties Relevant for Deep Geothermal Projects

Paul Hardegger, Hans R. Schneider, Reto Schnellmann

Introduction

The success of any extracting method to harvest geo-energy is heavily dependent on the wellbore stability. Well costs are by far the highest in the construction of a deep geothermal plant and the wellbore short- and long-term stability is crucial for operational as well as financial reasons.

The mechanical properties of the rock are fundamental parameters as they determine to a great extent the stability of a wellbore. However, for in-situ stresses and temperatures encountered in deep geothermal harvesting (borehole depths of 8’000 m and temperatures from ambient to about 250° C), reliable constitutive rock properties are largely missing.

Laboratory studies on rock samples have shown that an increase in temperature has a significant effect on the mechanical properties of the rock. Laboratory tests on rock samples indicate that high temperatures result in a significant reduction in peak strength as well as in a reduction in the deformation characteristics. However, the combined effects of high pressures and high temperatures on the mechanical behavior of rock as encountered in deep boreholes, relevant for geothermal projects, is fundamentally missing.

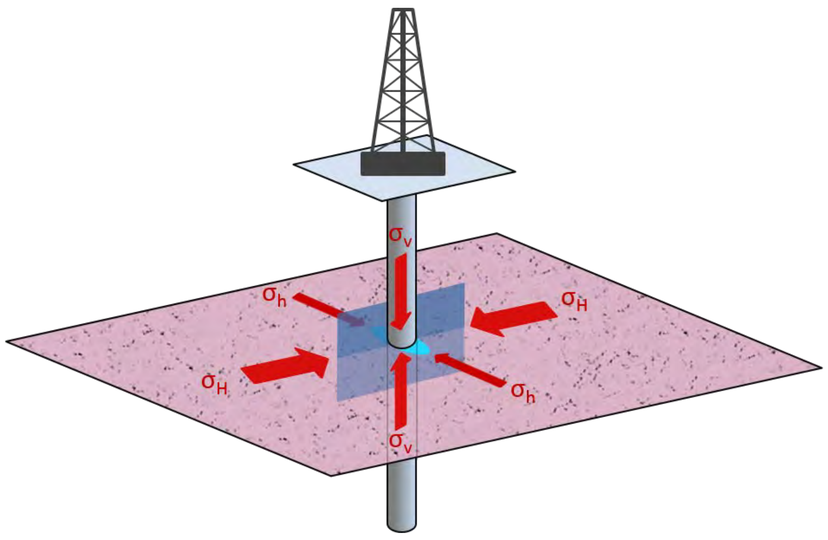

Fig. 1: Development of fracture plane and wellbore breakouts

Objectives

The objective of this project is the physical determination of rock properties at high stresses and corresponding high temperatures encountered in deep geothermal harvesting. In addition, constitutive models to describe the rock properties at relevant pressure and temperature conditions faced in deep geothermal boreholes will be developed to further analyze the deformation behavior of deep boreholes.

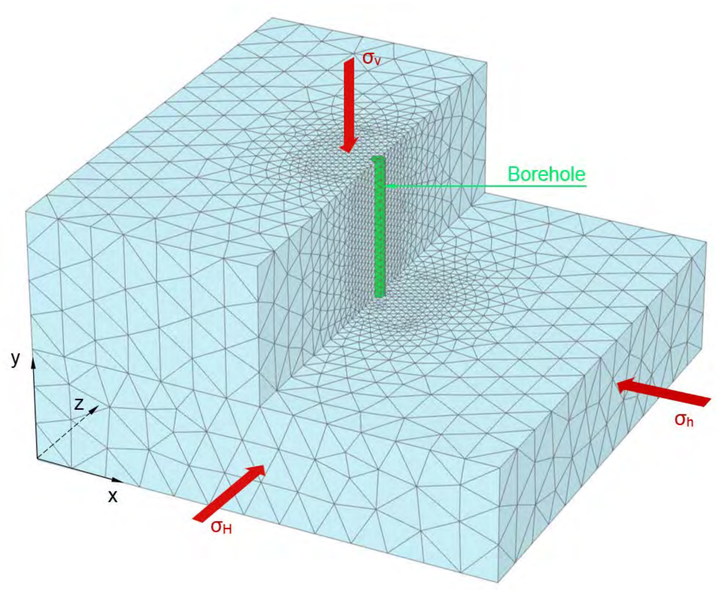

Fig. 2: Numerical analysis of wellbore stability

Methods

Laboratory experiments with a custom-made high pressure and high temperature triaxial equipment will provide the fundamental information for the improvement of constitutive rock properties required for a comprehensive assessment of deep borehole stability.

Based on laboratory tests under conditions relevant for deep geothermal harvesting (i.e. high pressure combined with high temperature), existing failure criteria will be improved to account for the combined effects of high pressures and high temperatures. Special emphasis is placed on polyaxial failure criteria derived from axisymmetrical triaxial testing conditions. This allows for the incorporation of truly 3-dimensional constitutive relationships into numerical codes.

High pressure and high temperature triaxial system

The high pressure and high temperature triaxial equipment is a fully automated system specifically designed for testing a variety of materials under high pressure and temperature conditions. The main parts of the equipment consist of the load frame, a hydraulic cylinder and the triaxial cell including a heating mantle.

Vertical forces of up to 20’000 kN can be applied either displacement or load controlled. The triaxial system is constructed such that temperatures of up to 220° C can be applied simultaneously with confining pressures of up to 200 MPa. The triaxial cell accommodates cylindrical samples of up to 70 mm.

The system allows a variety of different test sequences to be performed. A real time data acquisition system allows the continuous monitoring of the various measurements during testing. The system is also equipped with an ultrasonic device to measure P- and S-waves vertically as well as radially.

Fig. 3: High pressure and high temperature triaxial system

SCCER SoE
SWISS COMPETENCE CENTER for ENERGY RESEARCH
SUPPLY of ELECTRICITY

SCCER-SoE Annual Conference 2016

In cooperation with the CTI
Energy
Swiss Competence Centers for Energy Research
Schweizerische Eidgenossenschaft
Confédération suisse
Confederazione Svizzera
Confederaziun svizra
Swiss Confederation
Commission for Technology and Innovation CTI

Investigation of chemical stimulation of geothermal reservoirs using reactive flow-though system

Jin Ma, Xiang-Zhao Kong, Martin O. Saar*

Geothermal Energy and Geofluids, Institute of Geophysics, ETH Zurich, Switzerland
** Email: jin.ma@erdw.ethz.ch*

Introduction

Within recent years, many (European and other) sites have been investigated to determine if they are suitable for economic geothermal energy utilization. For example, the next planned geothermal power plant site in Switzerland, Haute-Sorne, is an EGS project. Permeability may be increased by hydraulic, thermal, and/or acid stimulation techniques. Acid treatment is a preferred method to enhance flow performance near wells (Portier et al., 2009) as the risk of inducing seismicity is low. However, stimulation-induced (or natural) porosity changes affect reservoir permeability in highly complex ways. In order to optimize this process, it is important to investigate the evolution of porosity, permeability and reactive surface area of the rocks under reactive flow-through conditions.

To delineate these coupled processes, hydrothermal flow-through experiments on rock cores (i.e. core-flooding) is one of the state-of-the-art approaches allowing us not only to examine relevant chemical reactions due to mineral dissolution and precipitation, but also to provide critical insights into permeability evolution (Fig. 1) and associated changes in fluid, solute, and heat transfer.

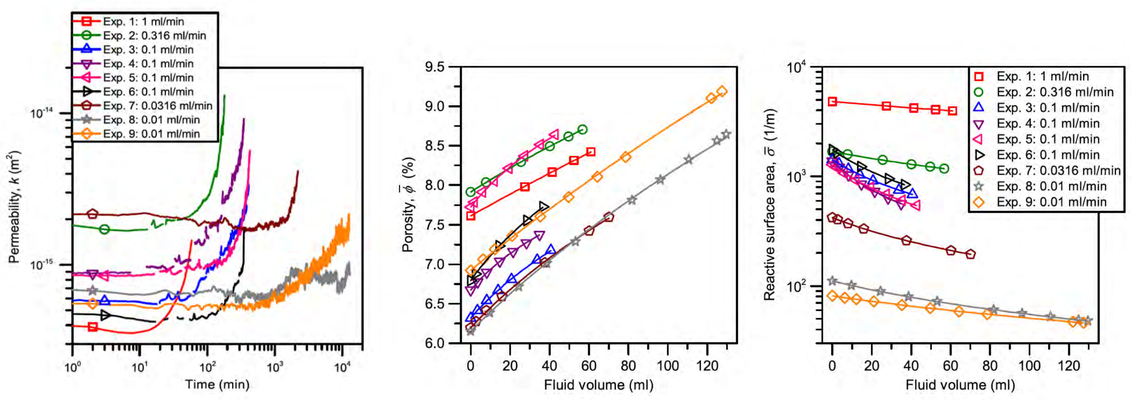

Fig.1 Evolution of permeability, porosity and specific reactive surface area observed in CO_2-charged brine injection in dolomite rock cores at a working temperature of 100 °C and pressure of 150 bar. (after Luhmann et al., 2014)

Samples and Methods

We are collecting core samples from different geothermal sites (Klaipeda, Vydmantai and Palange in Lithuania, shown in Fig.2), and will perform a series of detailed laboratory analysis, including

- ✓ Mineral composition analysis
  - X-ray powder diffraction (XRD)
  - X-ray fluorescence (XRF)
  - Scanning electron microscope (SEM) - Wavelength-Dispersive X-ray Spectroscopy (WDS) / Energy Dispersive X-ray Spectroscopy (EDS)
  - Microscopy
- ✓ Specific & Reactive surface area
  - Scanning electron microscope (SEM) - Backscattered electrons
  - Brunauer-Emmett-Teller (BET)
  - Reactive flow experiments
- ✓ 3D structure visualization
  - Micro-CT
- ✓ Pore size distribution analysis
  - Barrett-Joyner-Halenda (BJH)
- ✓ Porosity & permeability changes
  - Reactive flow experiments
- ✓ Reaction rates
  - Reactive flow experiments

Fig.2 Geothermal sites in Lithuania.

Table 1 Chemical composition of two sandstone samples

Oxide (wt%)	Sample 1	Sample 2
SiO_2	55.218	72.668
TiO_2	0.282	0.366
Al_2O_3	3.159	5.280
Fe_2O_3	3.212	2.051
MnO	0.174	0.068
MgO	6.730	3.211
CaO	11.262	4.739
Na_2O	0.040	0.088
K_2O	1.142	1.957
P_2O_5	0.020	0.036
Cr_2O_3	0.004	0.006
NiO	0.001	0.001
LOI	18.234	8.598
Total	99.476	99.069

Table 1 provides an XRF analysis on the oxide mass fraction of the Samples 1 and 2, from site Palanga (981.0 m deep) and site Vydmantai (954.6 m deep) in Lithuania, respectively.

Reactive flow-through experimental set-up

We are currently setting up the flow-through system which works in both recycling and single-pass modes.

- Recycling mode: for reactions approaching equilibrium
- Single-pass mode: for reactions far-from-equilibrium

The system can go up to 100 MPa and 200 ℃ with brine/CO_2-enriched brine as working fluid, which can represent most of the geothermal reservoir conditions.

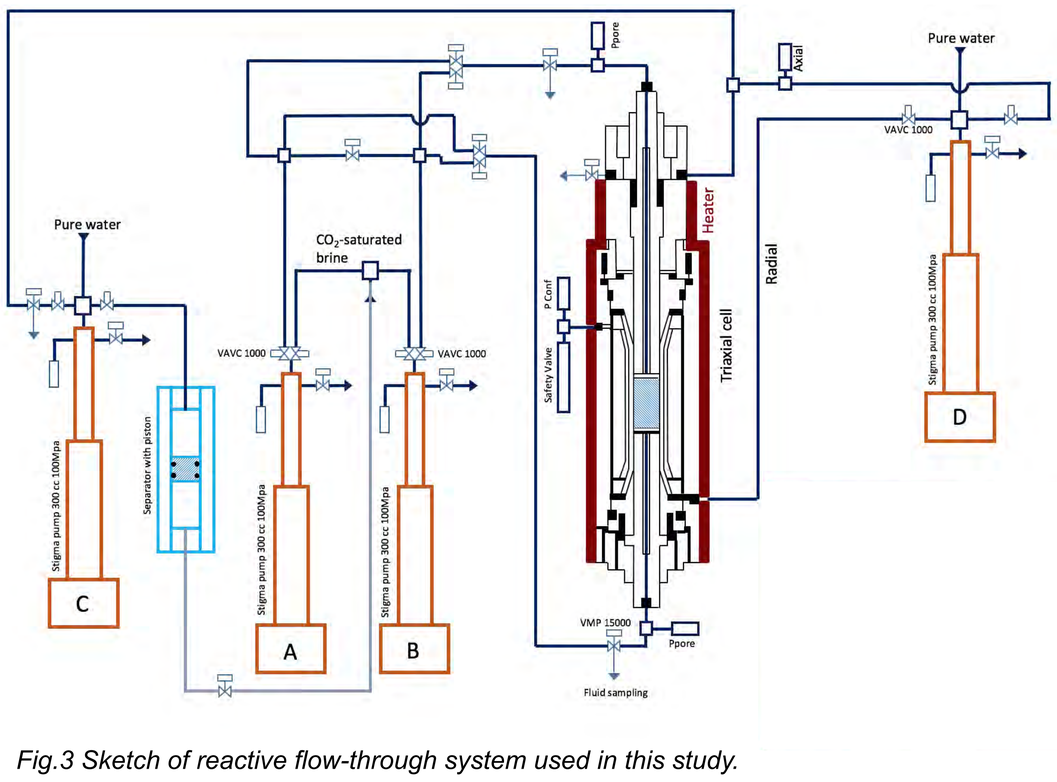

Fig.3 Sketch of reactive flow-through system used in this study.

References

Luhmann, A.J., X.-Z. Kong, B.M. Tutolo, N. Garapati, B.C. Bagley, M.O. Saar, and W.E. Seyfried Jr., Experimental dissolution of dolomite by CO2-charged brine at 100ºC and 150 bar: Evolution of porosity, permeability, and reactive surface area, Chemical Geology, 380, 145-160, 2014.

Portier, S., Vuataz, F.-D., Nami, P., Sanjuan, B., & GŽrard, A. (2009). Chemical stimulation techniques for geothermal wells: experiments on the three-well EGS system at Soultz-sous-Forts, France. Geothermics, 38(4), 349-359.

Acknowledgement

The project is funded by the European Union's Horizon 2020, "DESTRESS" under grant No. 691728.

DESTRESS
Geothermal Energy & Geofluids
ETH
Eidgenössische Technische Hochschule Zürich
Swiss Federal Institute of Technology Zurich

SCCER SoE
SWISS COMPETENCE CENTER for ENERGY RESEARCH
SUPPLY of ELECTRICITY

SCCER-SoE Annual Conference 2016

In cooperation with the CTI
Energy
Swiss Competence Centers for Energy Research
Schweizerische Eidgenossenschaft
Confédération suisse
Confederazione Svizzera
Confederaziun svizra
Swiss Confederation
Commission for Technology and Innovation CTI

Numerical simulation of the feasibility of ultra-deep, single-well geothermal power production

Thomas Driesner, ETH Zurich

Motivation

A swiss-based private company pursues the project to extrapolate their patented, open-hole approach for heat probes (several hundred meter depth with a supposed superior efficiency compared to conventional closed probes) to ultra-deep (nearly 9 km) wells for geothermal power production.
The company predicts stable production temperatures of ca. 150 - 155°C at circulation rates of 35 kg/s with reinjection at 70°C, equivalent to 12.8 MW_{th}.
In a study for the Swiss Federal Office of Energy I simulated the transient evolution of such systems. Simulations clearly show that the projected thermal power will not be reached and the well will cool rapidly to production temperatures well below 100°C. Ultra-deep, single-well geothermal power production is unlikely to be economic.

Methods & Model Setup

The system was simulated with the USGS software HYDROTHERM, by 2D simulations in cylindrical coordinates. The company interprets the superior efficiency of their heat probes as being the results of a damage zone surrounding the borehole that leads to a negative skin effect, i.e., enhances the effective borehole diameter.

This effect was modelled by a cylindrical zone surrounding the borehole with a diameter given by the company. The skin zone was given a very high thermal conductivity in order to simulate a best case scenario. Model validation was obtained by comparison with published simulations and by comparison with heat probe production data provided by the company.

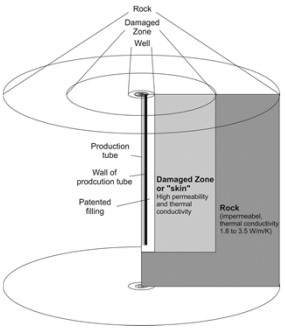

Production Temperature Evolution.

For the projected circulation rate and reinjection temperature, the production temperature rapidly decreases to below 100°C and nearly stabilizes below 90°C (solid red line).

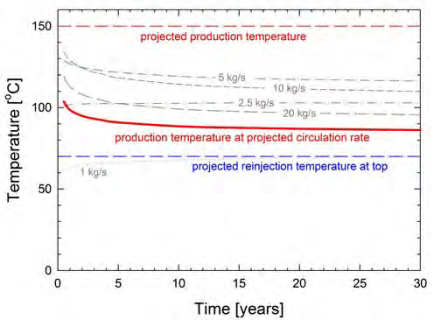

The reason is the poor thermal conductivity of the rock, leading to rapid cooling as the extracted heat cannot be conducted fast enough through the rock. The projected extra surface area due to the skin effect is insufficient to compensate for this.
The result shows only minimal sensitivity to changes in material parameters and diameter of the skin.

What Thermal Power is Possible?

In the best case and even for very large diameters of the damage / skin zone, the maximum thermal power is less than 20% of the projected one.

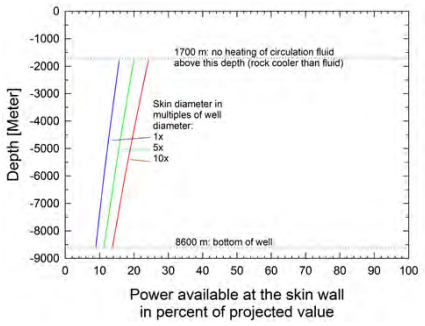

What Production Temperature is Possible?

The optimal production temperature is reached at a circulation rate of ca. 7 kg/s but is still significantly lower than the projected 150 - 155°C. Again, this points to less than 20% than the predicted thermal power.

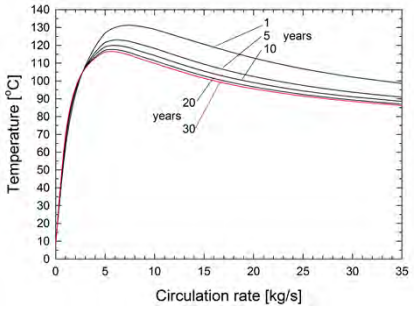

Adiabatic Heating/Cooling Effects

Upon flowing down, water pressure increases and water will adiabatically cool while it will get heated upon upflow. These effects are normally negligible but not for a 8.6 km vertical flow. However, they do compensate in a cycle and do not change the overall result.

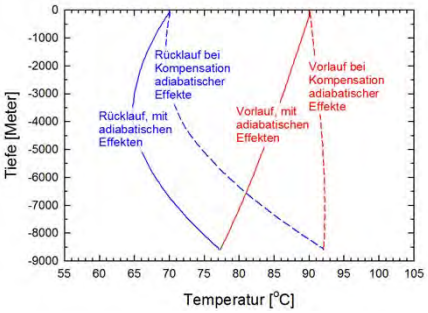

Conclusion

Due to fast cooling of the rock, significant power production from ultra-deep, single-well installations does not seem feasible with current economy and conversion technology.

SCCER SoE
SWISS COMPETENCE CENTER for ENERGY RESEARCH
SUPPLY of ELECTRICITY

SCCER-SoE Annual Conference 2016

In cooperation with the CTI
Energy
Swiss Competence Centers for Energy Research
Schweizerische Eidgenossenschaft
Confédération suisse
Confederazione Svizzera
Confederaziun svizra
Swiss Confederation
Commission for Technology and Innovation CTI

Numerical simulation of CO_2 injection into the Upper Muschelkalk aquifer, N. Switzerland: insights into fluid–rock reactions in the aquifer and at the contact to an overlying clay formation

Peter Alt-Epping, Larryn W. Diamond
Institute of Geological Sciences, University of Bern

1. Introduction

A study by (Chevalier et al., 2010) has identified several deep saline aquifers in the Swiss Molasse Basin, which may potentially be useful as reservoirs to store anthropogenic CO_2. One of these aquifers is the Trigonodus Dolomite of the Upper Muschelkalk formation. Predictive numerical modelling, constrained by in-situ testing and laboratory measurements, constitutes an important step in the evaluation of the storage capacity, injectivity and the long-term isolation performance of the aquifer. We use the reactive transport code PFLOTRAN (*www.pflotran.org*) to assess the implications of the dynamics of the CO_2 plume, fluid-fluid and fluid-rock interaction and pressure and temperature conditions for the safe, long-term storage of CO_2.

2. CO_2 plume migration, fluid-rock interaction and chemical trapping

Model design

- axisymmetric
- Injection rate: 50000 t /year

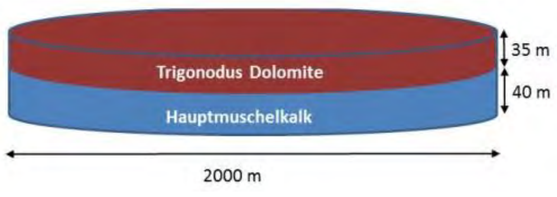

Fig. 1: Model domain

ROCK PROPERTIES		
	Trigonodus Dolomite	**Hauptmuschelkalk**
van Genuchten α	1.85e-5	1.85e-5
van Genuchten λ	0.6	0.6
Max. cap. pressure (Pa)	1e7	1e7
Residual saturation liquid	0.2	0.2
Residual saturation gas	0.05	0.05
Init. liquid saturation	1.0	1.0
Permeability (m^2)	1e-15	5e-17
Porosity	15%	5%
Dispersivity (m)	0.0	0.0
Thermal conductivity	2.51	2.51
Specific heat ($Jkg^{-1}°C$)	900	900

2.1 Effect of aquifer permeability on solubility trapping

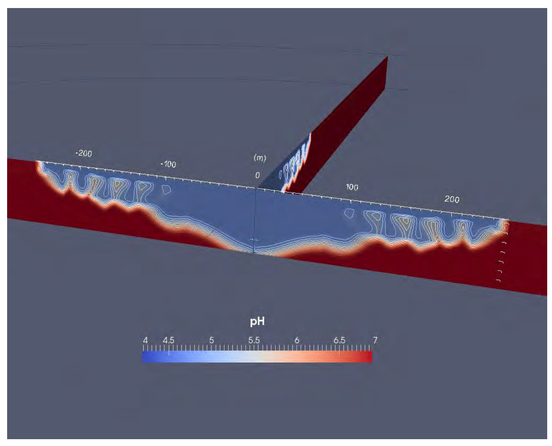

Fig. 2: The CO_2 pume after 5000 years shown as a region of low pH. Note the Finger-like downward convection of CO_2-enriched brine.

Fig. 3: In homogeneous aquifers the efficiency of CO_2 dissolution into the brine is a function of the aquifer permeability and porosity (panel A). The higher the permeability, the larger the plume/brine contact area and the faster CO_2 dissolves into the brine. Panel B shows the amount of CO_2 released into the brine as a result of carbonate mineral dissolution. The amount increases with permeability.

ROCK COMPOSITION		
Mineral	**Trigonodus Dolomite**	**Hauptmuschelkalk**
Calcite	5%	75%
Dolomite	74%	14%
Anhydrite	2%	6%

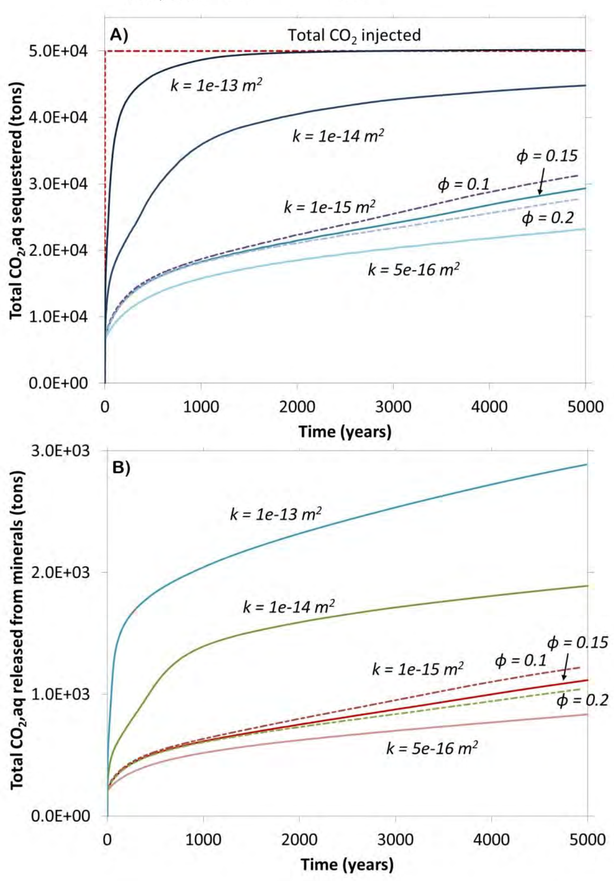

2.2 Release of metal contaminants into the brine

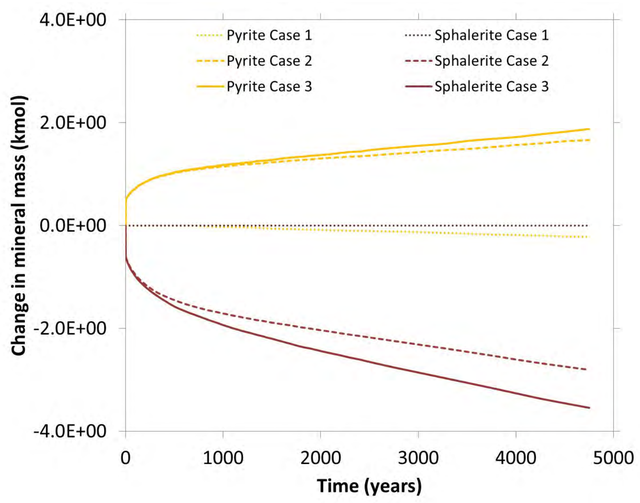

Fig. 4: Change in global mineral mass

Small amounts of primary pyrite and sphalerite are added to the rock. Sphalerite dissolves while pyrite precipitates, releasing Zn^{2+} into the brine.

Simulation cases:
Case 1: base case without CO_2 injection.
Case 2: injection into a rock without primary siderite
Case 3: injection into a rock with primary siderite

3. Reactive transport processes at the aquifer/clay interface

We address the issue of seal integrity by using a generic model of an interface between a carbonate aquifer and a clay rock. We simulate the arrival of a CO_2 plume and look at the reactive transport processes taking place on both sides of the interface by using a new transport module that combines diffusive transport with electro-migration to take into account the effect of the surface charge of clay minerals on solute transport.

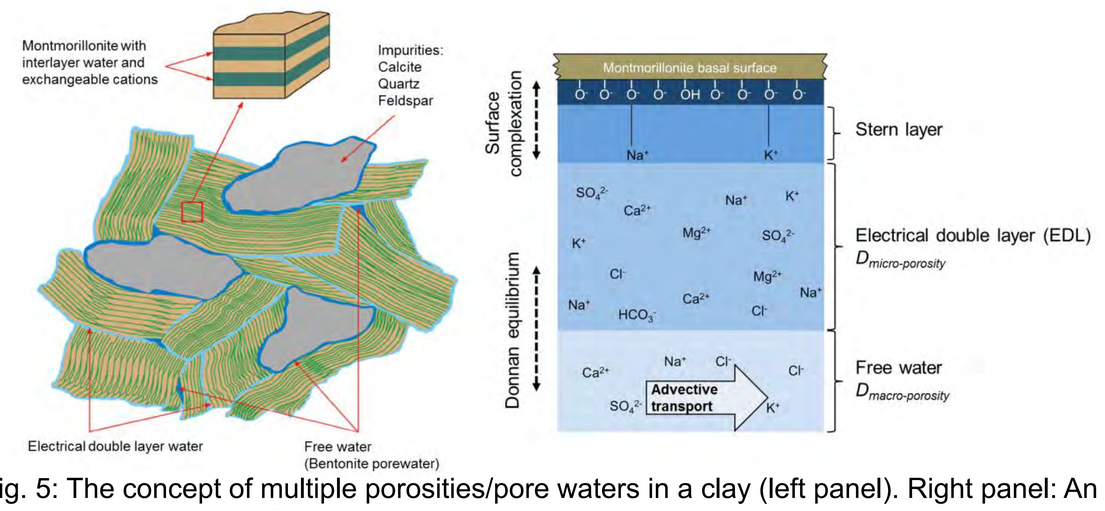

Fig. 5: The concept of multiple porosities/pore waters in a clay (left panel). Right panel: An electrical double layer (EDL) forms at clay mineral surfaces balancing their negative surface charge. Away from the surface, the water is no longer affected and internally charge balanced (from Alt-Epping et al., 2014)

3.1 A new approach to model reactive transport in clay

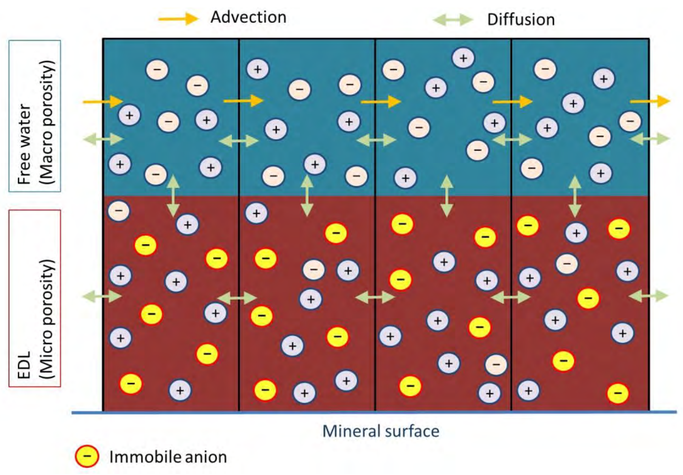

The new approach simulates the surface charge of clay minerals as immobile anions in the EDL. The Nernst-Planck equation is then used to simulate diffusive transport and electro-migration such that local charge balance is attained.

Fig. 6: Concept model of ion transport in a clay using immobile anions

3.2 Comparison between EDL and conventional ion exchange

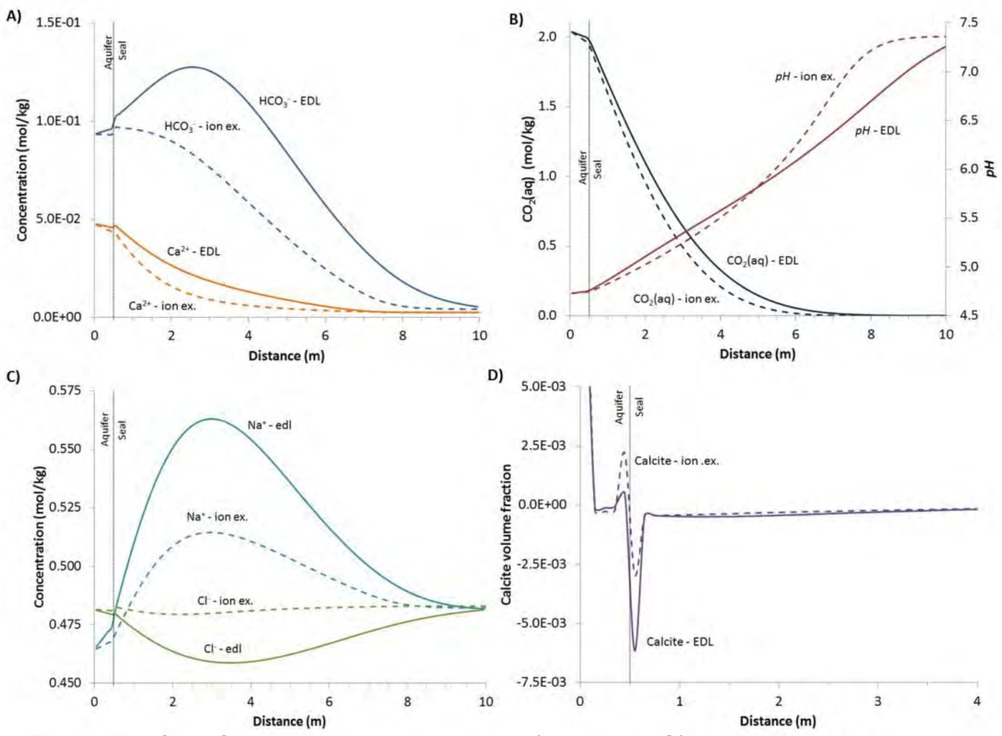

Fig. 7: Profile of pore water composition (panels A-C) and calcite volume changes (panel D) across the aquifer/clay seal interface.

4. Conclusions

- The efficiency of CO_2 solubility trapping increases with permeability
- Carbonate minerals dissolve, releasing additional CO_2 into the brine
- The amount of CO_2 released from minerals increases with permeability
- There is a risk that metal contaminants are released into the brine
- A new transport module accounting for electrical double layers in clay predicts strong calcite dissolution in a clay seal

References

Alt-Epping P, Tournassat C, Rasouli P, Steefel CI, Mayer KU, Jenni A, Mäder U, Sengor SS, Fernandez R, Benchmark reactive transport simulations of a column experiment in compacted bentonite with multispecies diffusion and explicit treatment of electrostatic effects. Comp. Geosci.2014; doi:10.1007/s10596-014-9451-x..

Chevalier, G., Diamond, L.W., Leu, W. (2010) Potential for deep geological sequestration of CO2 in Switzerland: a first appraisal. Swiss Journal of Geoscience 103: 427-455.

SCCER SoE

SWISS COMPETENCE CENTER for ENERGY RESEARCH
SUPPLY of ELECTRICITY

ETH zürich

DESTRESS

SCCER-SoE Annual Conference 2016

Towards modeling geochemical effects on long-term permeability evolution and heat extraction

In cooperation with the CTI

Energy
Swiss Competence Centers for Energy Research

Schweizerische Eidgenossenschaft
Confédération suisse
Confederazione Svizzera
Confederaziun svizra

Swiss Confederation

Commission for Technology and Innovation CTI

Julian Mindel and Thomas Driesner, Institute of Geochemistry and Petrology, ETH Zurich

Abstract / Background

This poster is a progress report on our work on coupling a combined the revised CSMP++ flow simulation platform [1] with the GEMS3K [2] chemical equilibration code. The current state includes implementations in terms of OpenMP parallelism, heat transport, and creation of a higher-level modular re-usable code design.
This work is a further step towards modeling reactive transport with realistic representations of discrete networks of thin fractures in large porous rock masses. Understanding the interaction of coupled processes such as mineral precipitation and dissolution, fluid flow, thermal effects, buoyancy, and mechanics is key for risk assessment and planning of Enhanced Geothermal Systems (EGS).

Methodology & key progress

Modeling thermal transport in such systems (EGS) in a computationally efficient way while neglecting the least amount of process detail –often highly non-linear-- is a well known challenge. The approach we have followed honors the algorithm proposed in [5]. Through operator splitting and a sequential solution approach we assume conductive heat transfer to take place mainly through rock while advective heat transport happens in the fluid. The resulting thermal-compressive effects are coupled to mass transport via a *mass correction source term*. A major advantage of implementing this solution approach is that it has already been implemented in a multi-phase context for a slightly different discretization approach [5], and thus leaves the door open for extended features in the current single phase simulator while being coupled to GEMS3K [2]. Figures 1 and 2 present sample test simulations in 2D, and 3D respectively.
The implementations above were carried out following a C++ code design pattern. The basic inheritance diagram is shown in Figure 3a. For the C++ oriented, Simulator is an *Abstract* class that inherits from *mix-in* classes that provide useful reusable functionality. Any simulator class can thus inherit from the Simulator class and use its functions to build an algorithm and perform a simulation. By creating such a design, underlying base functionality of CSMP++ is reused on subsequent versions of the same or new simulators. When an upgrade/improvement happens in the base functionality, all simulators are simultaneously upgraded with no or minimal need for modifications. Furthermore, there is also less need for training new users on CSMP++ core functionality.
As a further improvement, and given that the resulting THC simulator is expensive CPU-wise, we have worked on the parallelization of a number of operations, with particular emphasis on the chemical calculations. OpenMP directives have been implemented, and thus simulations may take advantage of this in shared memory systems. Sample speed-up results are presented in Figure 3b.

Outlook

We are currently still working towards adopting the CSMP++ “split node” approach [4] for reactive transport. In this approach, nodes at material boundaries are duplicated to allow an accurate calculation of fluid flow transport (although likely applicable to other processes as well) across material interfaces, in particular between fractures and matrix rock.
We are also planning for CSMP++ native MPI functionality to be implemented for simulations on distributed memory systems (i.e. clusters). The existing MPI functionality used by the simulator developed in this work stems from the SAMG iterative solver package developed at Fraunhofer SCAI, and hence could certainly use an improvement to become more efficient and scalable.

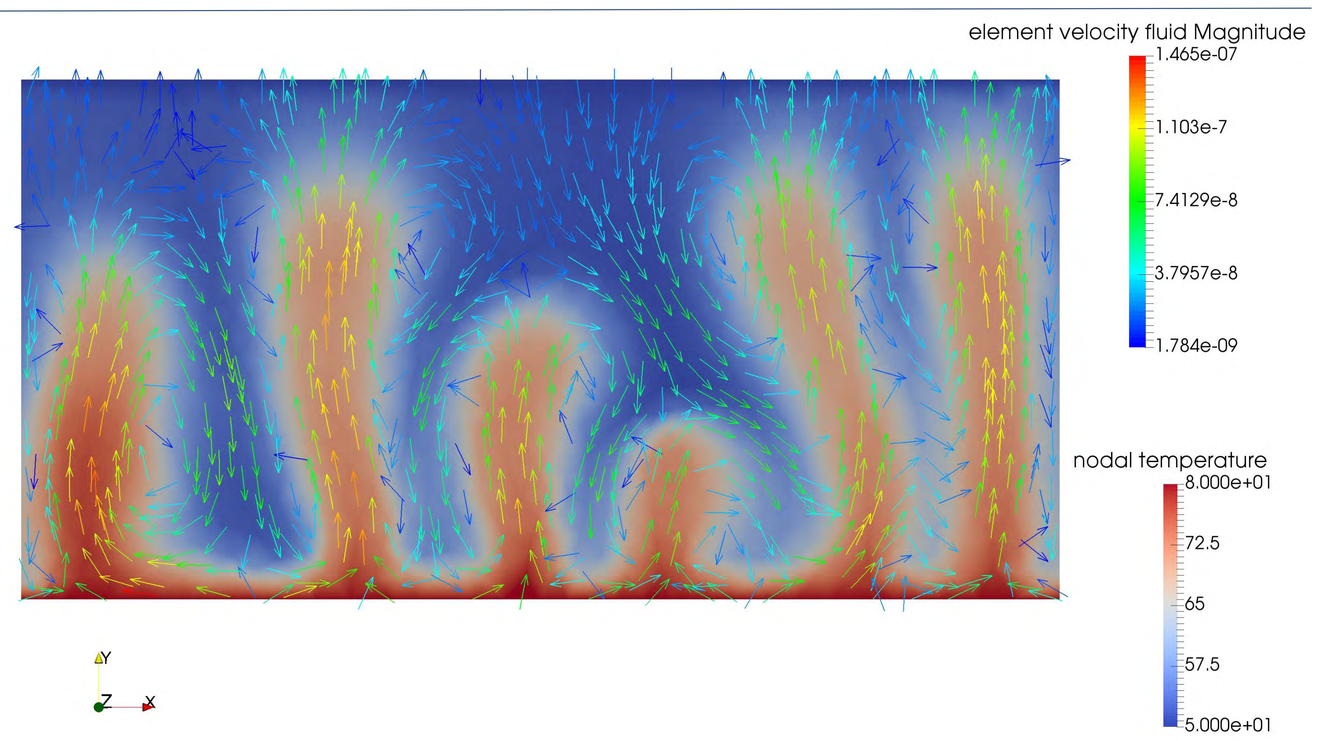

Figure 1: Two dimensional test simulation of hydrothermal flow throw porous media. Heat is provided through the bottom boundary causing convective plumes to appear. Heat transport is modelled through the algorithm proposed in [5]

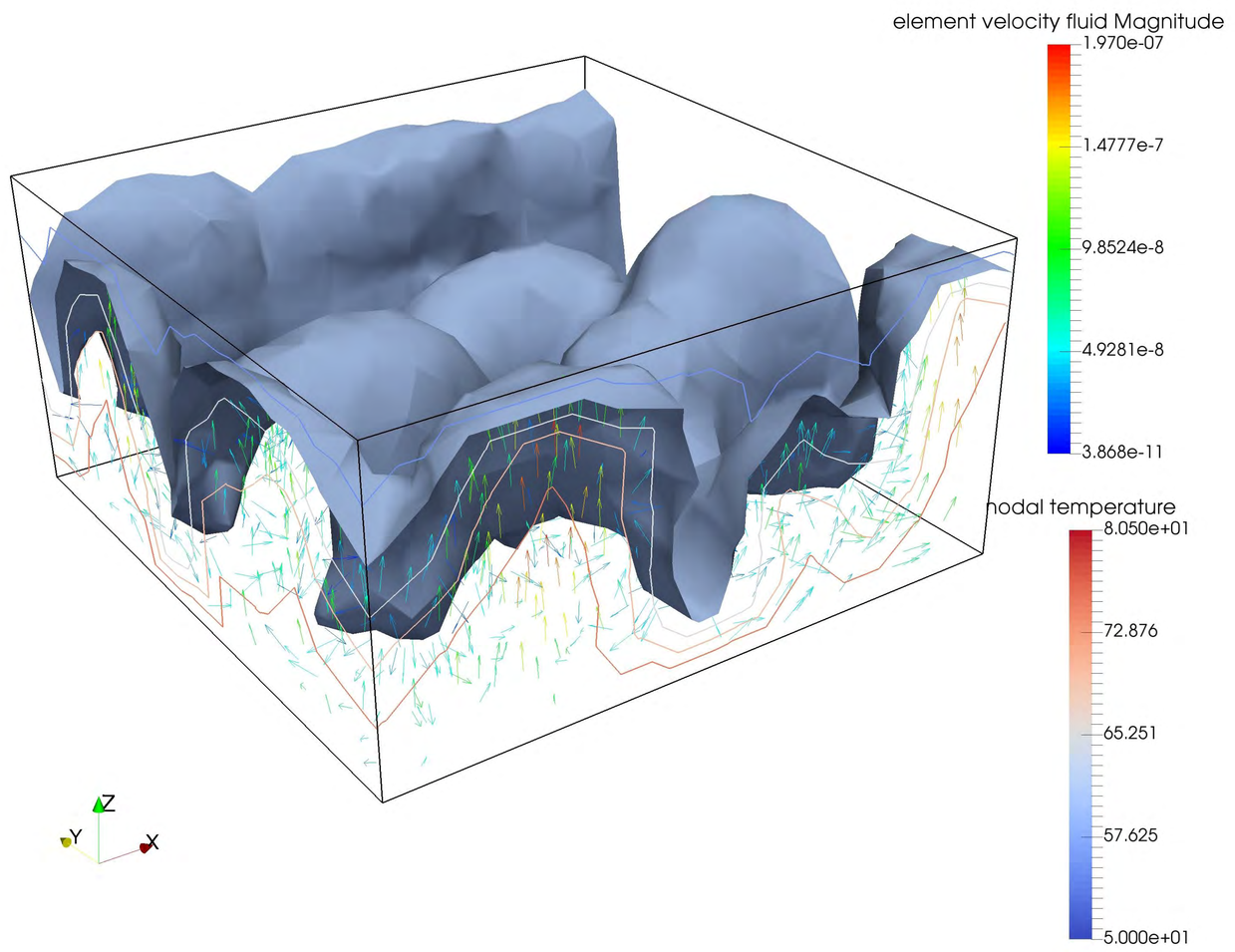

Figure 2: Three dimensional test simulation of hydrothermal flow throw porous media. Heat is provided through the bottom boundary causing convective plumes to appear. Heat transport is modelled through the algorithm proposed in [5]

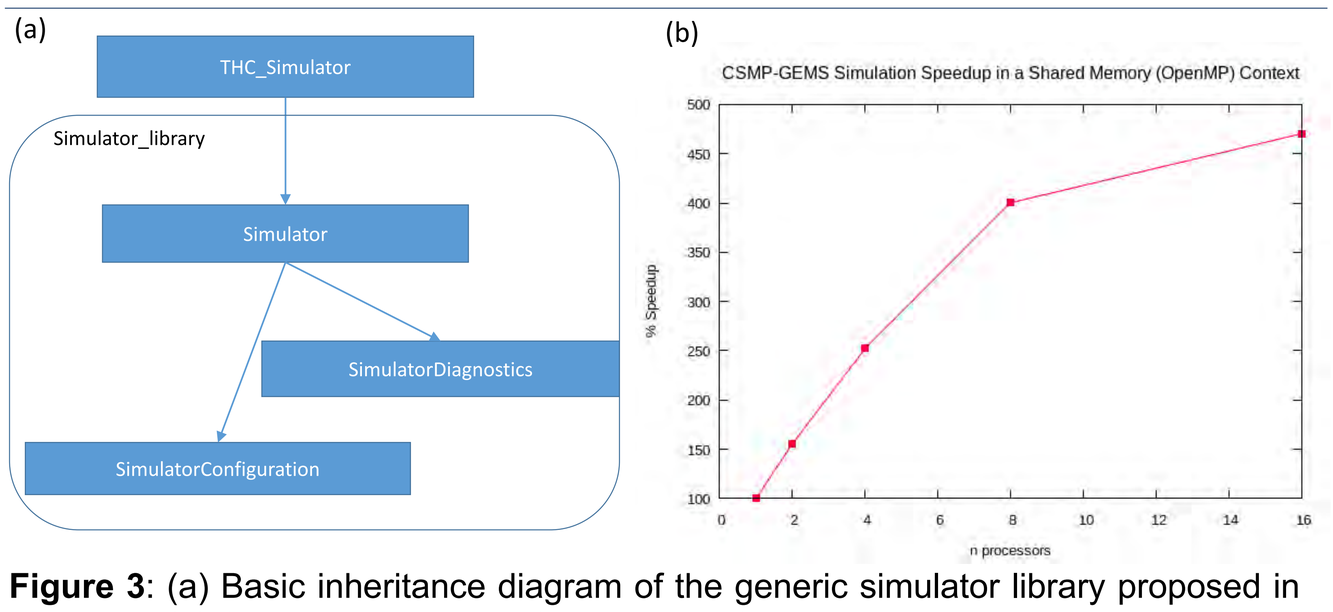

Figure 3: (a) Basic inheritance diagram of the generic simulator library proposed in this work. (b) Speed-up diagram of a sample HC calcite dissolution [3] simulation on a 3D test domain with 40000 tetrahedrons.

References

1. Matthai S.K. et al. (2012) ECMOR XIII, European Conf. Mathematics of Oil Recovery, Biarritz, France;
2. Kulik D.A. et al. (2013) Computational Geosciences 17,1-24; 3
3. Engesgaard, P., Kipp, K.L. (1992) Water Resour. Res. 28, 2829–2843; 4
4. Nick H.M. and Matthai S.K. (2011) Vadose Zone Journal 299-312
5. Weiss, P. et al. (2014) Geofluids 14, 347-371, 3

SCCER SoE

SWISS COMPETENCE CENTER for ENERGY RESEARCH
SUPPLY of ELECTRICITY

Geothermal Energy & Geofluids

SCCER-SoE Annual Conference 2016

Development of efficient numerical methods and codes for geochemical modeling and reactive transport calculations with applications in geothermal energy and carbon sequestration in geological formations

In cooperation with the CTI

Energy
Swiss Competence Centers for Energy Research

Schweizerische Eidgenossenschaft
Confédération suisse
Confederazione Svizzera
Confederaziun svizra

Swiss Confederation

Commission for Technology and Innovation CTI

Philipp Schaedle[1], Allan M.M. Leal[1] , Anozie Ebigbo[1], Nagasree Garapati[2], Martin O. Saar[1]
[1] ETHZ, Institute of Geophysics, Geothermal Energy and Geofluids
[2] West Virginia University

Introduction

The efficient computational simulation of multiphase-multicomponent fluid flow coupled with geochemical reactions in porous and/or fractured subsurface systems is essential for the successful assessment of many energy-related applications. Examples of such applications include:

1) Carbon dioxide storage in geologic formations
2) Geothermal energy extraction
3) Combinations of 1) & 2), i.e. CO_2-Plume Geothermal (Randolph and Saar, 2011)
4) Radioactive waste disposal
5) Groundwater protection and contaminant transport

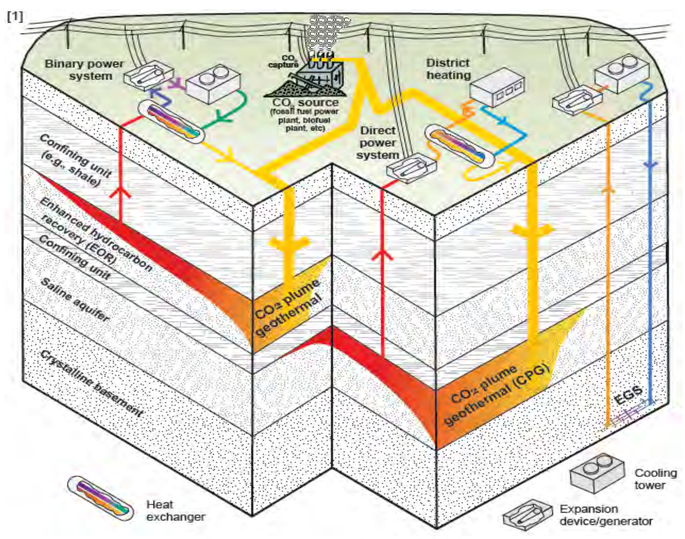

Randolph and Saar, 2011

Computational & physical challenges:

- wide variety of coupled physical and chemical processes
- changes in rock porosity and permeability as a result of mineral dissolution and/or precipitation

Tools

- Utilization of state-of-the-art numerical tools, namely FEniCS (fenicsproject.org) and Reaktoro (reaktoro.org)
- Coupling with other backends for the calculation of both thermodynamic and thermophysical properties of rock minerals and fluids.

FEniCS

- FEM — Unstructured meshes
- Adaptive mesh refinement — Convenient tools are provided
- Many sparse linear solvers — **Example:** PETSc, UMFPACK
- Massively parallel calculations — Convenient tools are provided
- Wide range of FEM schemes — **Example:** continuous and discontinuous Lagrange, (discontinuous) Raviart-Thomas etc. **Of special interest in porous media flow**
- Fast and efficient implementation of computer codes for the simulation of complex physical phenomena

Reaktoro

- Efficient, robust and accurate methods for chemical equilibrium and kinetics calculations — Leal et al., 2015, 2016a,b,c
- Numerical methods for reaction modeling especially developed for performance-critical applications — **Example:** reactive transport modeling
- Modern numerical optimization methods are applied to the solution of the chemical equations used for the calculation of thermodynamic properties of rock minerals and fluids (brine and gases) as functions of temperature, pressure, and composition

Approach

Coupling of a FEniCS-based flow and transport solver with our chemical reaction simulator, Reaktoro.

FEniCS - solve governing partial differential equations

- Pressure & velocity (Mixed-hybrid-finite element method) — Lagrange space: saturation & pressure; Discontinuous Raviart-Thomas: velocity
- Heat transport: Conduction, Convection
- Mass transport: Advection, Diffusion, Dispersion

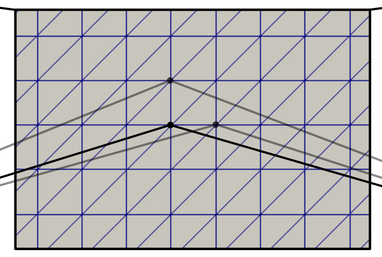

Equilibrium calculation at every node of the mesh at every time step

Reaktoro - geochemical calculations

- Equilibrium Calculations — **Example:** equilibrate 1kg H_2O, 1 mol NaCL, 100 g CO_2. **What is the molar amount of each species? What phases are stable in equilibrium?**
- Reaction Path Calculations — **Example:** react 100 g of a mineral (e.g., calcite) in a CO_2-saturated brine for a day. **How does the amount of calcite change with time? What about the concentration of CO_2 and other ions?**
- Speciation Calculations — **Example:** given concentrations of some elements, pH, and other conditions, calculate the amount of each species. **What minerals are super/under- saturated?**
- Thermodynamic Property Calculations — **Example:** standard molar properties (e.g., Gibbs energies, enthalpies, volumes) using SUPCT databases and Helgeson (HKF) equations of state
- Thermophysical Property Calculations — **Example:** Fluid (mixture) viscosity & heat capacity

CoolProp - thermodynamic/ thermophysical properties

Current status

- Implementation of single-phase flow simulator
- Implementation of two-phase flow simulator
- Simulation of simple two-phase flow cases
- Verification of two-phase code

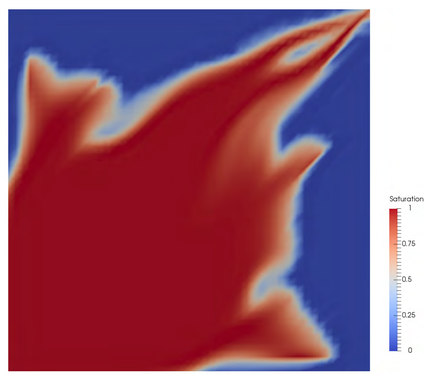

Saturation field of water (blue) in oil (red); flow from lower left to upper right corner; simulated with our preliminary two-phase flow solver

Outlook

- Implement adaptive mesh refinement
- (Further) verification and improvement of the two-phase code (e.g., compressible fluids, saturation - capillary pressure relationships)
- Implementation of transport equations (solutes and heat)
- Coupling to geochemical simulator
- GPU enabled geochemical simulator

References

Randolph, J. B., & Saar, M. O. (2011). Coupling carbon dioxide sequestration with geothermal energy capture in naturally permeable, porous geologic formations: Implications for CO2 sequestration. Energy Procedia, 4(May), 2206–2213. http://doi.org/10.1016/j.egypro.2011.02.108
Leal, A. M. M., Blunt, M. J., & LaForce, T. C. (2015). A chemical kinetics algorithm for geochemical modelling. Applied Geochemistry, 55, 46–61. http://doi.org/10.1016/j.apgeochem.2014.09.020
Leal, A. M. M., Kulik, D. A., & Kosakowski, G. (2016). Computational methods for reactive transport modeling: A Gibbs energy minimization approach for multiphase equilibrium calculations. Advances in Water Resources, 88, 231–240. http://doi.org/10.1016/j.advwatres.2015.11.021
Leal, A. M. M., Kulik, D. A., & Saar, M. O. (2016). Enabling Gibbs energy minimization algorithms to use equilibrium constants of reactions in multiphase equilibrium calculations. Chemical Geology, 437, 170–181. http://doi.org/10.1016/j.chemgeo.2016.05.029
Leal, A. M. M., Kulik, D. A., Kosakowski, G., & Saar, M. O. (2016). Computational methods for reactive transport modeling: An extended law of mass-action, xLMA, method for multiphase equilibrium calculations. Advances in Water Resources, 96, 405–422. http://doi.org/10.1016/j.advwatres.2016.08.008

SCCER-SoE Annual Conference 2016

SCCER SoE
SWISS COMPETENCE CENTER for ENERGY RESEARCH
SUPPLY of ELECTRICITY

In cooperation with the CTI
Energy
Swiss Competence Centers for Energy Research
Schweizerische Eidgenossenschaft
Confédération suisse
Confederazione Svizzera
Confederaziun svizra
Swiss Confederation
Commission for Technology and Innovation CTI

Hydromechanical aspects of CO_2 breakthrough and flow in clay-rich caprock

Roman Makhnenko, Danila Mylnikov, Victor Vilarrasa, and Lyesse Laloui
Soil Mechanics Laboratory – chair «Gaz Naturel» Petrosvibri, École Polytechnique Fédérale de Lausanne

1. Introduction

Research of the chair "Gaz Naturel" – Petrosvibri at the EPFL contributes to SCCER-SoE task 1.2: "Reservoir modelling and validation". Both numerical modeling and experimental investigation of geomechanical processes involved in deep geological storage of CO_2 are performed in cooperation with government agencies: SFOE and Swisstopo. Proper assessment of carbon dioxide storage procedure allows to significantly reduce its concentration in the atmosphere and thus directly contributes to Swiss energy strategy 2050.

Deep saline aquifers have the greatest potential for geological storage of carbon dioxide and due to their worldwide occurrence can play a major role in reduction of carbon dioxide emissions. Injected CO_2 changes the local effective stresses and temperatures and thus can significantly deform the involved rock. One of the issues is the caprock integrity or possible CO_2 propagation through the rock layers overlying the reservoir formation. The ongoing experimental investigations involve oedometric tests, where carbon dioxide is injected in brine-saturated clay-rich caprock-like materials at different temperatures and pressures.

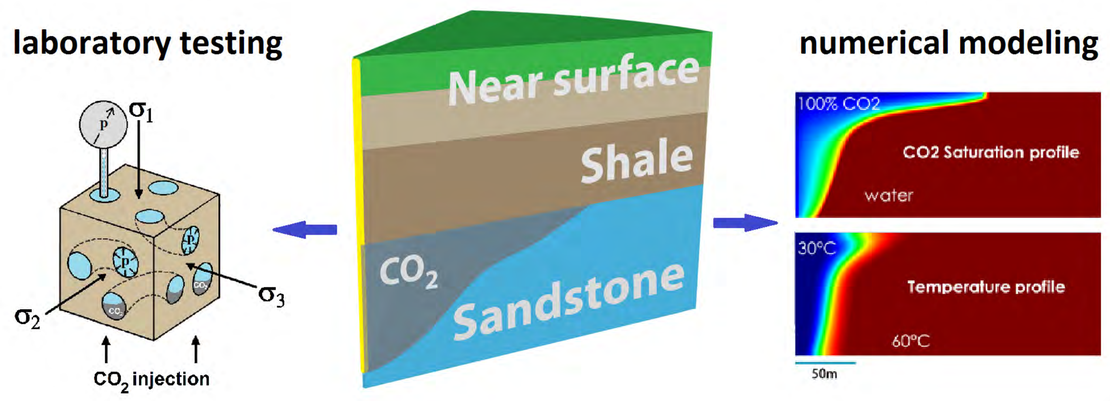

Fig. 1: Sketch of the LMS-EPFL research activities on geologic CO_2 sequestration.

2. Background and methods

CO_2 is usually injected in liquid state and, in sedimentary basins at depths below 800 meters, it changes its phase to supercritical fluid ($scCO_2$) with temperature above 31.1° C and pressure exceeding 7.4 MPa. Threshold capillary pressure p_c (Fig. 2) is an intrinsic property of each particular pore throat and for a cylinder of diameter d, γ - surface tension at the brine-CO_2 boundary and θ - contact angle of brine-CO_2 surface with respect to solid phase,

$$p_c = \max(p_{CO_2} - p_{brine}) = \frac{4\gamma\cos\theta}{d}$$

Breakthrough pressure is determined as the differential fluid pressure at which constant flow of CO_2 through the specimen was established, i.e., when CO_2 started to displace brine within the pore space.

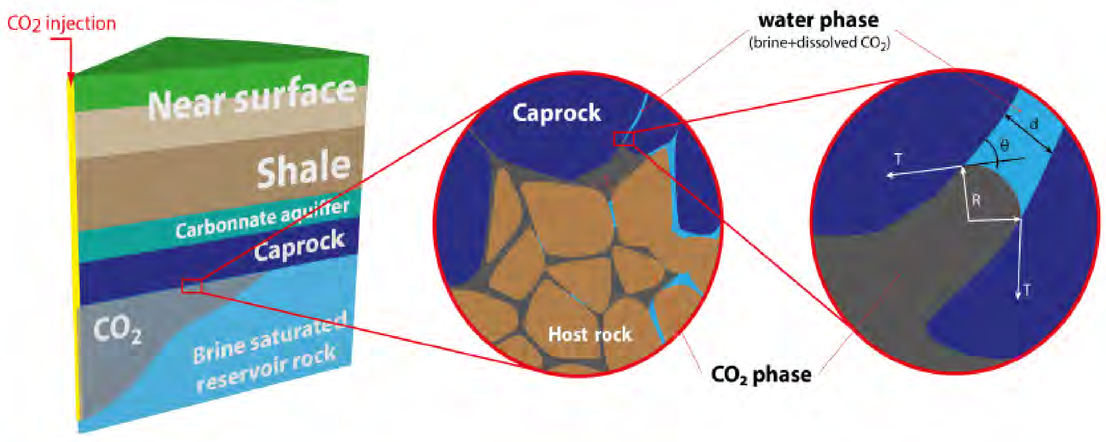

Fig. 2: Capillary effects at the reservoir-caprock interface.

CO_2 injection tests are performed on cylindrical specimens (height h = 12.5 mm diameter D = 35 mm) loaded in oedometric cell (Fig. 3). Liquid (24°C) and supercritical CO_2 (42°C) breakthrough and flow are studied in rock specimens fully saturated with brine with constant (8 MPa) downstream pressure.

After breakthrough occurs, viscous steady-state vertical Darcy flow of CO_2 through the material is assumed and effective CO_2 permeability is

$$k_{CO_2}^{eff} = \frac{4\Delta V_{CO_2}\eta_{CO_2}h}{\pi D^2 \Delta p_{diff}\Delta t}$$

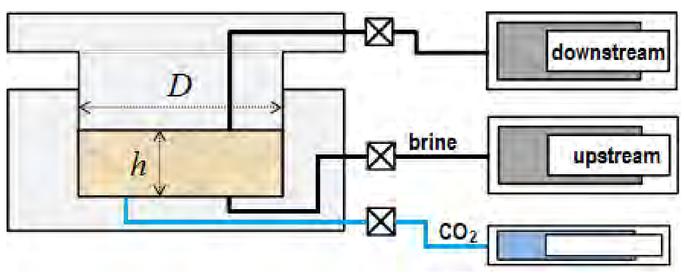

Fig. 3: Sketch of experimental setup.

3. Results and Discussion

Remolded (i. e., reconstituted) Opalinus clay specimens saturated with natural brine are tested. Loading to 35 MPa vertical stress and 8 MPa pore pressure provides full saturation and porosity of 0.13 with dominant pore throat diameter of 40 nm (Fig. 4).

The breakthrough pressure is measured using the direct method (Fig. 5), where excess CO_2 pressure is slowly and gradually increased until continuous CO_2 flow is observed (Thomas *et al.*, 1968). At every new level of differential pressure, more CO_2 dissolves in the pore fluid, but eventual decrease of CO_2 flow rate indicates that viscous flow is not actually established. After differential pressure increases to 4.2 MPa (at 35 MPa vertical stress), CO_2 flow rate reaches a constant level of approximately 5 mm^3/ hour, hence breakthrough is reported. Also, an indirect experimental technique (Hildenbrand *et al.*, 2002) is implemented: a capillary threshold pressure is measured as the differential fluid pressure (2.8 MPa at 35 MPa vertical stress in Fig. 6) when CO_2 stops flowing through the specimen after its injection is finished. CO_2 breakthrough pressure increases with effective mean stress, which is related to compression of the pores and reduction in pore throat diameters. Relationship between direct and indirect methods is to be analyzed further since the latter one usually provides smaller p_c values.

CO_2 effective permeability decreases with effective mean stress (Fig. 7) and increases with differential pressure because of the capillary effects: the higher the pressure – the larger is the amount of pores that participate to non-wetting fluid flow.

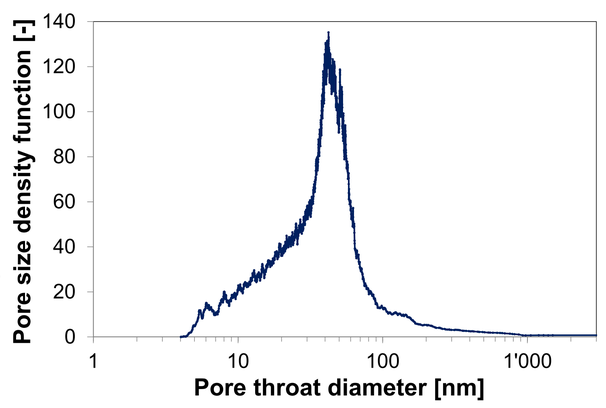

Fig. 4: Pore throat diameter distribution in remolded shale loaded to 35 MPa.

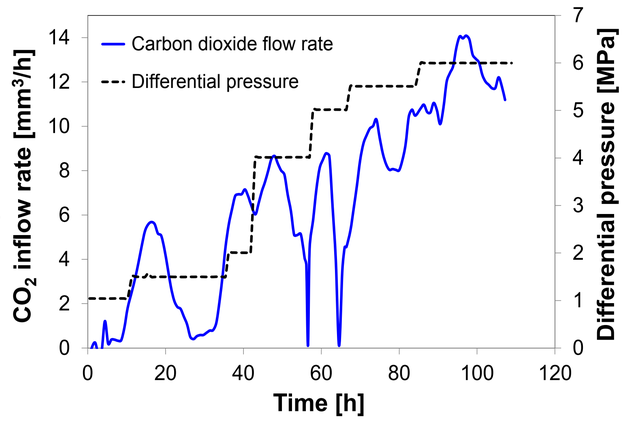

Fig. 5: CO_2 breakthrough pressure measurements using the direct method.

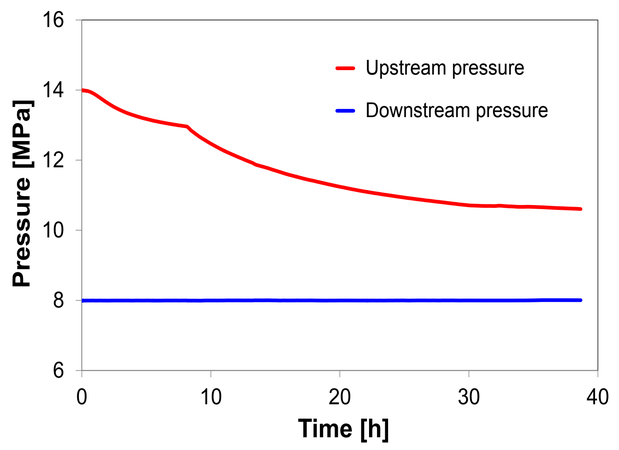

Fig. 6: Results of CO_2 breakthrough pressure measurements by the indirect method.

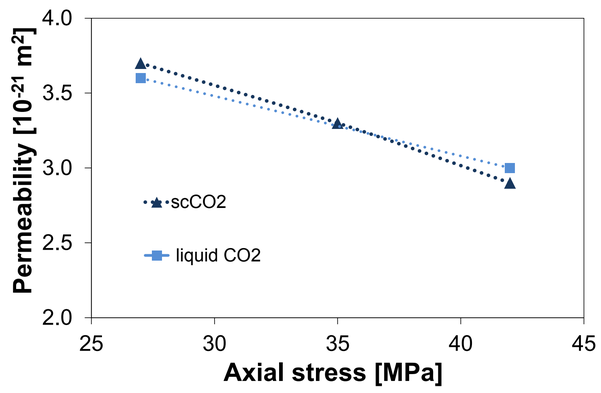

Fig. 7: Liquid and $scCO_2$ permeabilities of remolded shale vs applied axial stress.

4. Conclusions

In order to study the caprock behavior during deep geological carbon dioxide storage, liquid and supercritical CO_2 were injected in brine-saturated clay-rich material at 24°C and 42°C. CO_2 breakthrough pressure was determined to be increasing with effective mean stress and CO_2 effective permeability was observed to increase with differential fluid pressure. Preliminary studies on capillary threshold pressure show that it is usually smaller than the breakthrough pressure. The proper calculation of the latter one is of particular importance for evaluating maximum injection rates for CO_2 storage projects.

Acknowledgements

R. Makhnenko is an SCCER-SoE postdoctoral researcher. Tested shale is provided by Swisstopo and the conducted experiments are a part of SFOE sponsored project CAPROCK #810008154.

References

Hildenbrand, A., S. Schlömer, B.M Kroos, 2002. Geofluids, 2:3-23.
Thomas, L.K., D. L. Katz, M.R. Tek, 1968. SPE Journal, 243:174–184.

SCCER SoE
SWISS COMPETENCE CENTER for ENERGY RESEARCH
SUPPLY of ELECTRICITY

SCCER-SoE Annual Conference 2016

In cooperation with the CTI
Energy
Swiss Competence Centers for Energy Research
Schweizerische Eidgenossenschaft
Confédération suisse
Confederazione Svizzera
Confederaziun svizra
Swiss Confederation
Commission for Technology and Innovation CTI

The effect of pressure on $CaSO_4$ solubility in geothermal systems

Denis Zezin (Institute of Geochemistry and Petrology, ETH Zurich)

Introduction

Aqueous fluids in geothermal systems are mostly represented by the solutions of electrolytes. Besides being a heat transfer medium, upon changes of physicochemical conditions these fluids may affect dissolution of a country rock or become saturated promoting the precipitation of minerals, both in the aquifer and as scales on the pipe walls. Therefore these liquid solutions, their composition and properties control a fluid flow via porosity and permeability changes in host rocks and wells of geothermal systems.

Issues in modeling of mineral dissolution/precipitation processes:

- Detailed knowledge of the thermodynamic properties and behavior of components (e.g., electrolyte solutions).
- Temperature and pressure effects – currently data are limited to temperature dependence at water vapor saturation pressure only.
- Properties of complex mixtures reflecting composition of natural aqueous solutions – mostly not known, usually approximated to one major component.
- Thermodynamic properties of solutions containing sparingly soluble salts – not easily available since the data are scarce and cannot be obtained directly due to experimental and solubility limitations.

Therefore the motivation of this study was to find an approach for calculation of the properties of sparingly soluble salts, particularly at elevated temperatures and pressures typical for geothermal reservoirs.

Method

$CaSO_4$ can be a ubiquitous salt in geothermal systems characterized by low solubility in aqueous liquid solutions. Its solubility in water is retrograde and reaches as little as 10^{-4}-10^{-3} mol/kg at 200 °C, so the properties of this solute can't be experimentally measured with sufficient accuracy. The pressure dependence on the equilibrium reactions involving fluids can be evaluated from the basic thermodynamic relations. Thus, for solubility calculations, the pressure effects on the equilibrium constant of reactions and the activity coefficients of components are derived from the volumetric properties as follows:

$$\left(\frac{\partial lnK}{\partial P}\right)_T = -\frac{\Delta V^0}{RT} \qquad \left(\frac{\partial ln\gamma_i}{\partial P}\right)_{T,n} = -\frac{V_i^{ex}}{RT}$$

Using our recent systematic studies of the density of electrolyte solutions at elevated temperatures and pressures [1-3], a synthetic density (volume) of $CaSO_4$ was evaluated using Young's mixing rule from the measured properties of NaCl, $CaCl_2$ and Na_2SO_4 and their mixtures at temperatures from 25 to 250 °C and pressures up to 1 kbar. Density measurements for mixed electrolyte solutions were done using vibrating tube densitometer. The partial molar volume of $CaSO_4$ derived from fitted Pitzer's model was used for calculation of the pressure dependence of the activity coefficient of solutes and equilibrium constant of solubility reaction. This approach permits evaluation of the solubility of gypsum and anhydrite in deep geothermal systems.

Results

The effect of pressure on mineral solubility is attributed to changes in activity coefficients of components in a liquid and thermodynamic equilibrium constant. These changes can be evaluated for $CaSO_4$ solute in pure water solvent using a Pitzer model for the volumetric properties of solutes:

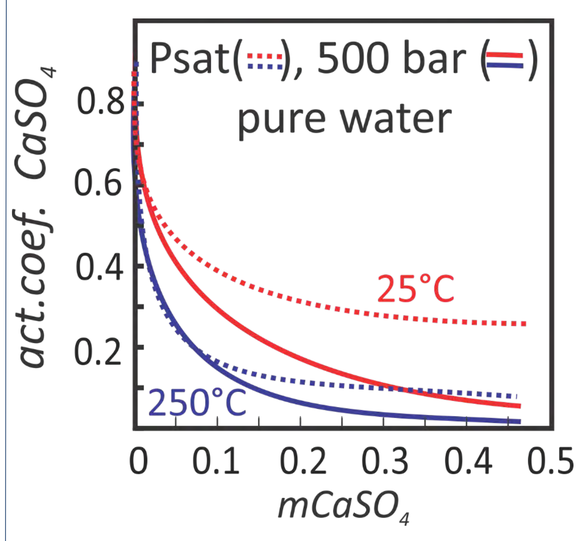

Figure 1. T- and P-dependence of the activity coefficient of $CaSO_4$ in water.

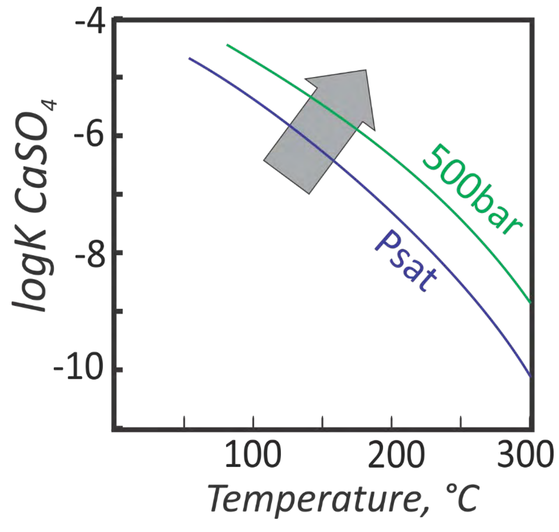

Figure 2. T- and P-dependence of the equilibrium constant for the solubility of $CaSO_4$ in water.

From these quantified effects it is possible to model the solubility of $CaSO_4$ (gypsum and anhydrite) in pure water:

$$CaSO_4 = Ca^{2+} + SO_4^{2-}$$

With addition of NaCl, the solubility of sulfate minerals significantly enhances. This is due to formation of stable pairs between ions of (Ca2+, Cl-) and (Na+, SO42-). The solubility can further be modeled:

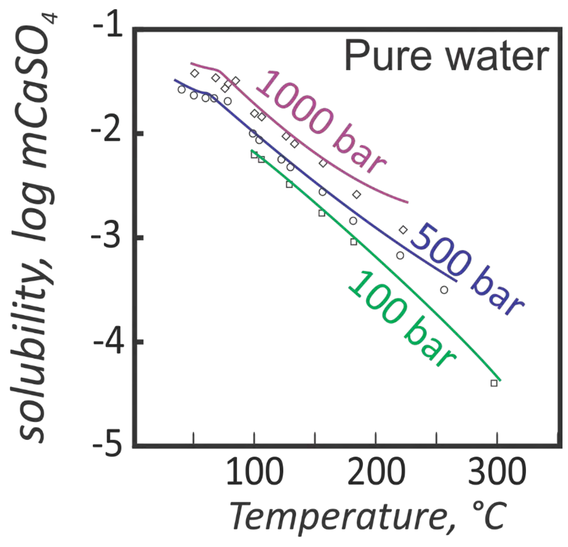

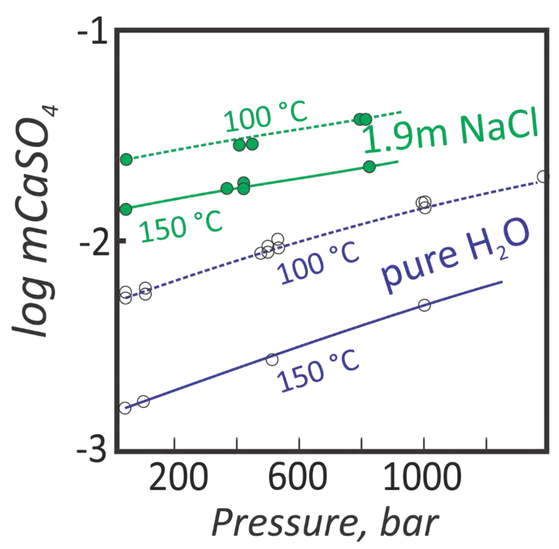

Figure 3 (left) and 4 (right). T and P controls on the solubility of $CaSO_4$ in water and NaCl solutions. Symbols are the experimental data from [4, 5].

Summary

Scaling is one of the major problems affecting permeability of a reservoir. Precipitation of the sulfates of calcium, barium and strontium may lead to a significant decrease in well productivity observed in many geothermal plants. Pressure controls on fluid-rock equilibrium can be evaluated from the volumetric measurements as show on the example of $CaSO_4$. The same approach can be used for calculation of the effect of pressure on the solubility of Ba and Sr sulfates.

References

[1] Zezin et al. (2014) J. Chem. Eng. Data 59, 736–749. [2] Zezin et al. (2014) J. Chem. Eng. Data 59, 2570–2588. [3] Zezin et al. (2015) J. Chem. Eng. Data 60, 1181–1192. [4] Blount and Dickson (1969) GCA 33, 227-245. [5] Blount and Dickson (1973) Am. Miner. 58,.323-331.

SCCER-SoE Annual Conference 2016

SCCER SoE
SWISS COMPETENCE CENTER for ENERGY RESEARCH
SUPPLY of ELECTRICITY

In cooperation with the CTI
Energy
Swiss Competence Centers for Energy Research
Schweizerische Eidgenossenschaft
Confédération suisse
Confederazione Svizzera
Confederaziun svizra
Swiss Confederation
Commission for Technology and Innovation CTI

Numerical modeling of seismic velocity dispersion and attenuation in 3D fractured media

Jürg Hunziker, Beatriz Quintal, Eva Caspari, Céline Mallet, Germán Rubino and Klaus Holliger; University of Lausanne

UNIL | Université de Lausanne

Introduction

For geothermal and hydrocarbon exploration as well as for nuclear waste and CO_2 storage it is crucial to retrieve information with regard to fractures within the subsurface region of interest. Seismic methods are suitable for this task, but, if the fracture thickness is significantly smaller than the wavelength, direct imaging is not possible. Fractures do, however, cause velocity dispersion and attenuation of the seismic signal due to wave-induced fluid flow (WIFF), which in turn may allow for an indirect characterization.

Several studies have investigated different aspects of WIFF using 2D modeling. However, to realistically mimic laboratory experiments or field scenarios, 3D simulations are necessary. The step from 2D to 3D is mathematically and physically relatively straightforward, but computationally quite cumbersome. Here, we present some basic 3D simulations to investigate the differences between 2D and 3D experiments in terms of the wave-attenuation as quantified by $1/Q_p$.

Method

We study WIFF in fractured media using numerical upscaling experiments to gain deeper insight into the rather complex physics at play. For P-waves, these numerical experiments consist of so-called compressibility tests, where a cubic sample under undrained conditions is compressed vertically along its upper boundary while the solid phase is neither allowed to have horizontal displacements at the lateral boundaries nor to have vertical displacements at the bottom boundary. Fractures are modeled as highly compliant and highly porous features embedded in a much stiffer and much less porous background. Solving the quasi-static poroelastic equations in the space-frequency domain with these boundary conditions allows for inferring the attenuation and velocity dispersion of a vertically propagating P-wave.

Results

Cube dimension: 0.4^3 m^3;
Fracture dimension: 0.2 m x 0.0001 m x D_y (D_y = fracture depth)

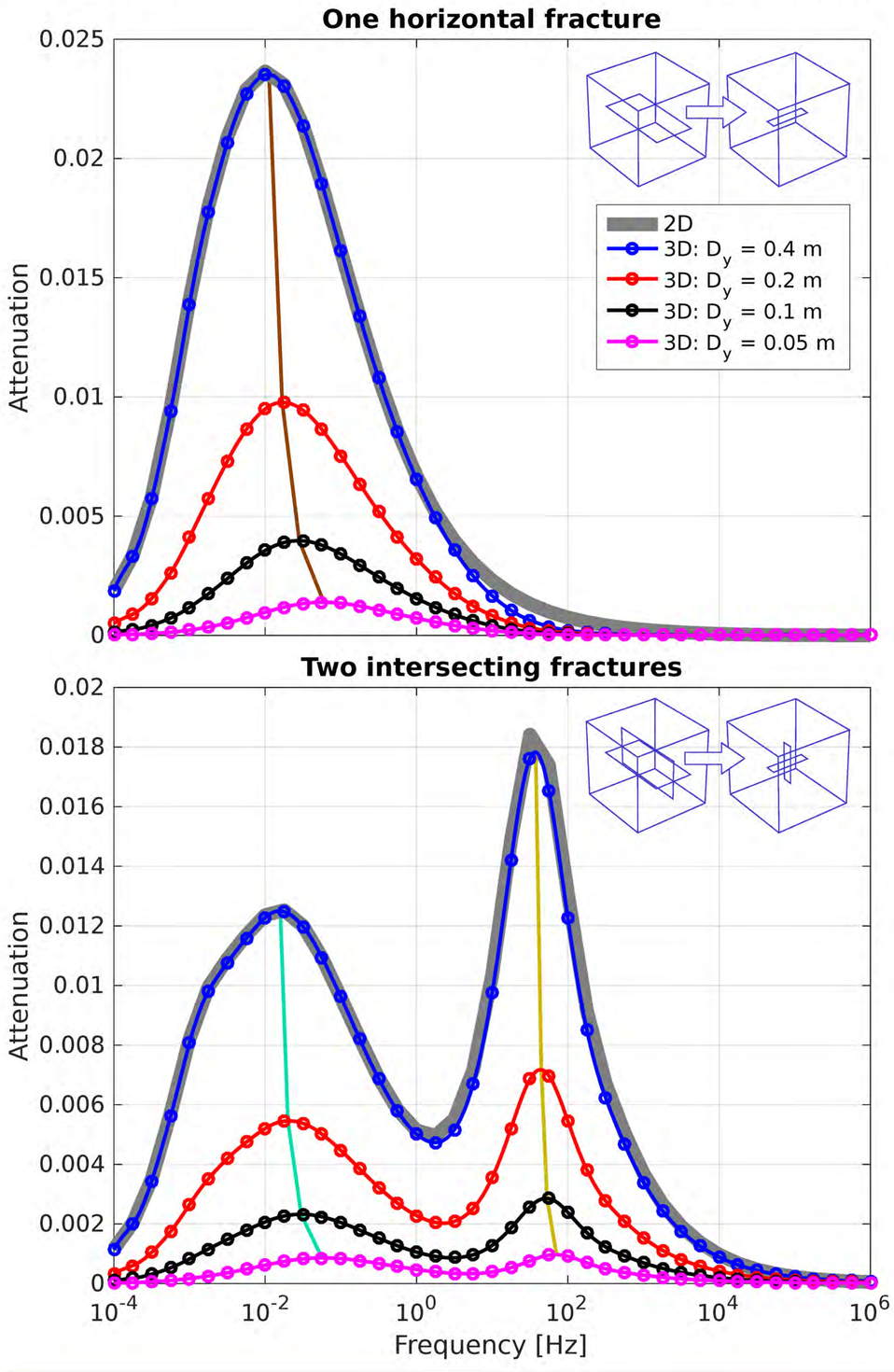

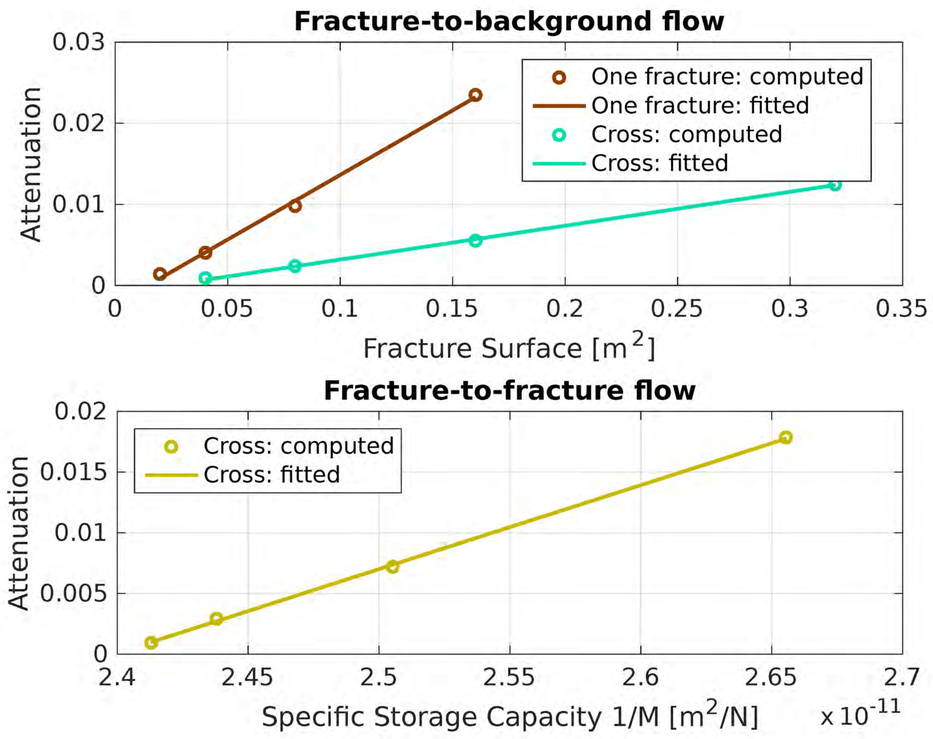

Results for weaker contrasts

Bulk modulus of dry frame K_b: 34e9 N/m^2 → 17e9 N/m^2
Shear modulus μ: 32e9 N/m^2 → 16e9 N/m^2

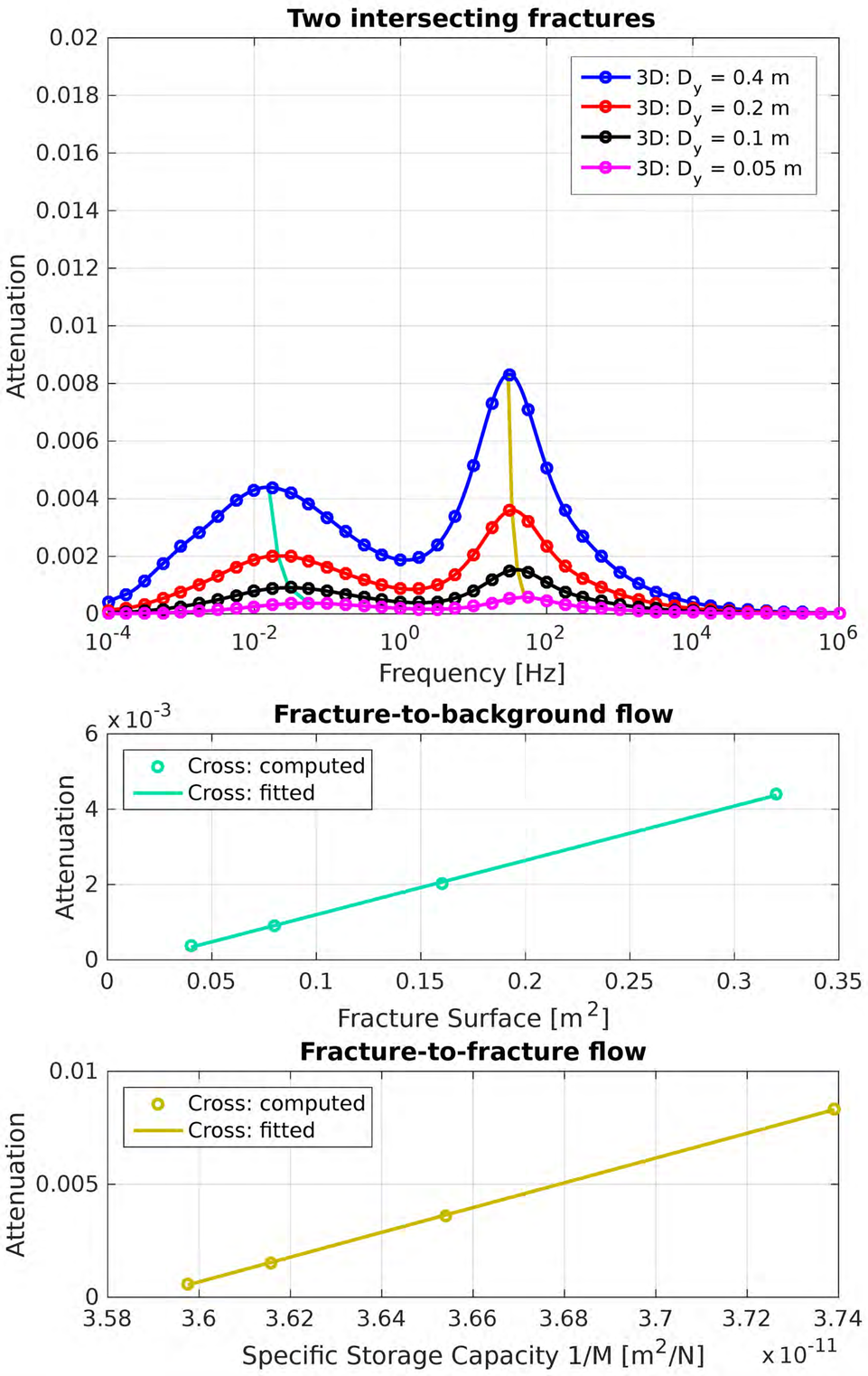

Conclusions

- The 3D nature of fractures affects WIFF considerably. Reducing the extent of the fractures in the third dimension (1) reduces attenuation due to WIFF and (2) shifts the characteristic frequency slightly towards higher frequencies.
- The relation between fracture extent, expressed as fracture surface or specific storage capacity, and the magnitude of the attenuation is linear for the cases investigated.

SCCER SoE

SWISS COMPETENCE CENTER for ENERGY RESEARCH
SUPPLY of ELECTRICITY

SCCER-SoE Annual Conference 2016

In cooperation with the CTI

Energy
Swiss Competence Centers for Energy Research

Schweizerische Eidgenossenschaft
Confédération suisse
Confederazione Svizzera
Confederaziun svizra

Swiss Confederation

Commission for Technology and Innovation CTI

Numerical Modeling of Natural Convection in Fractured Media

James Patterson, Thomas Driesner
Institute of Geochemistry and Petrology, ETH Zurich, Switzerland

Before EGS: In-situ Geothermal Gradient

Geothermal gradient is an important reservoir characteristic for a geothermal power project, dictating how deep a well must be drilled to reach a certain temperature and, therefore, well cost. However, faults and fractures in these rocks may facilitate natural convection: the process by which thermally-induced density differences of water cause cold, dense water to cycle deeper into the basement while hot, light water moves towards the surface. This can result in spatially varying temperatures around the upward/downward plumes. In Soultz-sous-Forêts, France the geothermal gradient in the first 1km of sedimentary cover is extremely high, ca. 100°C/km, and was assumed to continue into the granite basement. In reality, the next 3km of basement rock has a gradient of ca. 15°C/km, greatly reducing the actual bottom hole temperature. Pure conduction through the granite is insufficient to supply the heat flux measured in the cover; thus, natural convection within fractures is thought to cause the temperature anomaly. This research seeks to better understand the role of natural convection in fractures on temperature variations in the subsurface and its implications for geothermal energy.

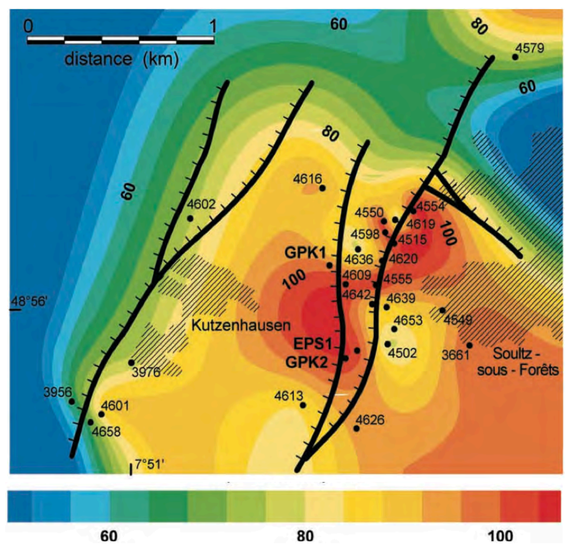

Temperature (°C) at 800m

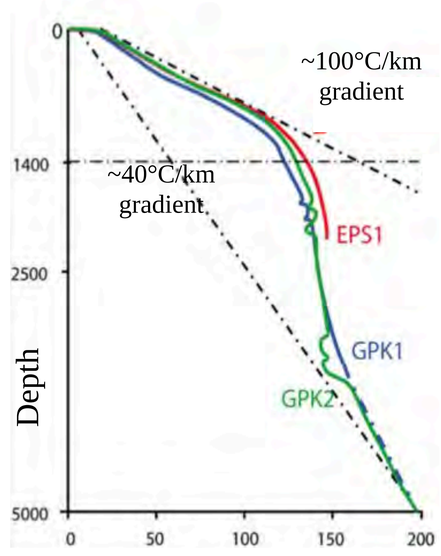

Temperature (°C)

Fig. 1 (left): *Measured and interpolated temperature at 800m depth; irregular shape distribution indicates convective plumes.*[1]
Fig. 2 (right): *Temperature profile to 5000m depth in 3 wells featured in Fig. 1. Sharp drop in gradient around 1400m due to impermeable layer blocking convection.*[2]

CSMP++ (Complex Systems Modeling Platform)

Simulations were performed using CSMP++, a reservoir modeling platform developed at ETH Zurich, Heriot-Watt University, Montanuniversität Leoben, and University of Melbourne. We employ operator splitting with both Finite Elements and Finite Volumes for diffusion and advection equations, respectively. Additionally, fluid properties are calculated using a pure water equation of state.

Natural Convection in a Single Fracture

In general, fracture dimensions and geothermal gradient determine whether or not natural convection will be initiated in a fracture. For a given fracture size and geothermal gradient, the fracture aperture determines whether natural convection is present and how many cells (connected regions of upward and downward flow) are present, as well as the strength/velocity of convection.

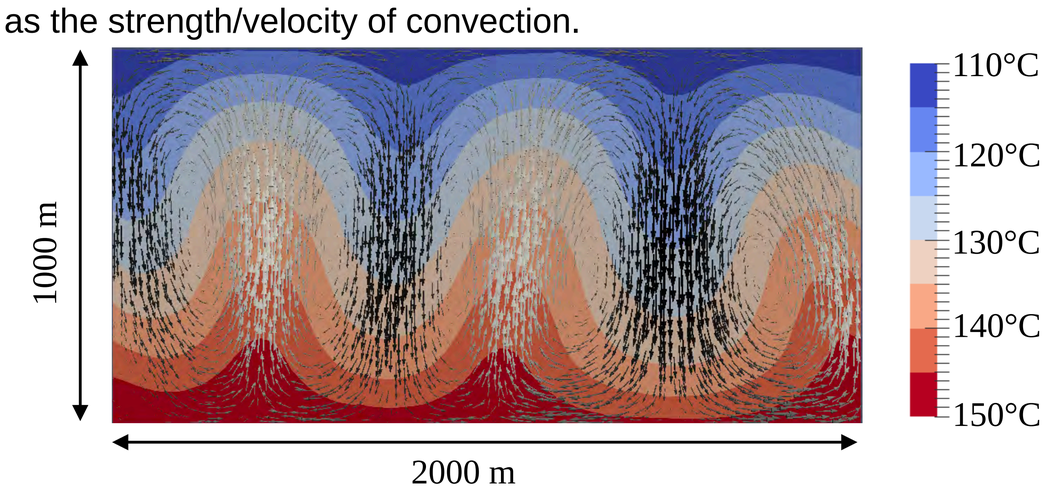

Fig. 3: *Fluid temperature and velocity arrows within single fracture with convection cells. White arrows indicate upward flow; black arrows indicate downward flow.*

Natural Convection in a Fracture Set

When multiple convecting fractures are in close proximity, temperature perturbations from each fracture influence the convection patterns in its neighbors. For example, an upward plume in one fracture creates a local hot spot, heating up part of a neighboring fracture, causing the fracture fluid to buoyantly rise. This "thermal connectivity" between fractures can initiate and/or strengthen convection in neighboring fractures. It also causes convection cells from multiple fractures to align along a common axis of rotation, resulting in convection "tubes." For parallel or en echelon fractures, this axis lies perpendicular or sub-perpendicular to the fracture strike. Thermal connectivity between convection cells also enhances the strength of convection, increasing the amount of fluid and heat transported.

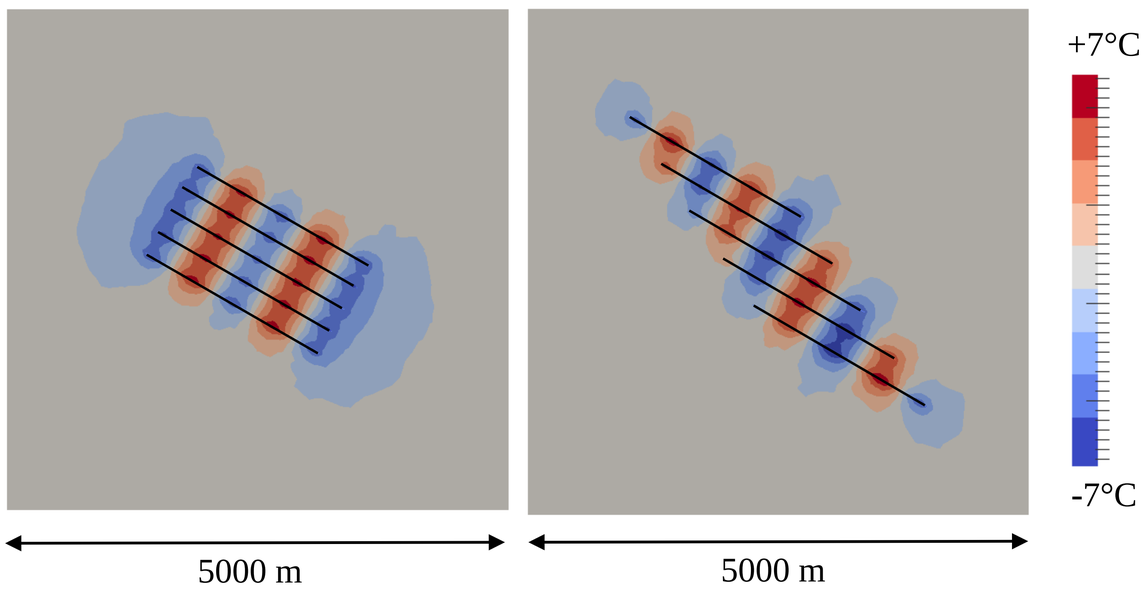

Fig. 4: *Bird-eye view of slice at 2500 m depth; 5 vertical, parallel fractures, spaced 250 m apart. Colored by temperature change due to natural convection. Left: no offset between fractures. Right: each fracture offset 500 m along fracture plane (en echelon).*

Natural Convection in two Fracture Sets

Rock units commonly contain multiple fracture sets with different orientations, creating a network of interconnected fractures. With two intersecting sets of parallel fractures with similar apertures, convection tubes form at an angle somewhere between the angles perpendicular to the strike of the two sets. In general, the orientation of the convective tube is influenced by the comparative strength of convection within the two sets, i.e. larger aperture or closer spacing. As the fracture network becomes more dense, convection tubes disappear and convection patterns begin to resemble those in porous and permeable reservoirs.

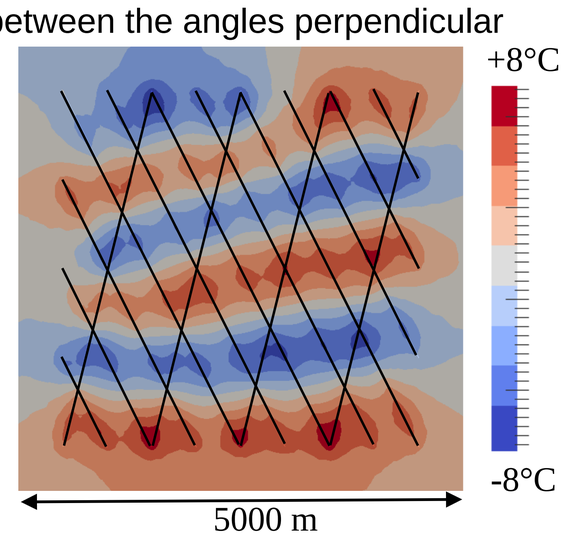

Fig. 5: *Bird's-eye view of slice at 2500 m depth; two intersecting fracture sets. Colored by temperature difference. Convection tubes form across fractures, regardless of fracture length.*

Conclusions and Future Work

Investigation into the fundamental role of natural convection within fractured media gives better understanding of geothermal reservoirs and may ultimately aid in site selection and well placement. By identifying the causes behind lateral temperature variations, reservoir models can more accurately simulate the subsurface and better predict the performance of a geothermal project.

References

[1] Clauser, C., Griesshaber, E., Neugebauer, H.J. (2002) Decoupled thermal and mantle helium anomalies: Implications for the transport regime in continental rift zones. Journal of Geophysical Research, Vol. 107.

[2] Siffert, D., Haffen, S., Garcia, M.H., Geraud, Y. (2013) Phenomenological study of temperature gradient anomalies in the Buntsandstein formation, above the Soultz geothermal reservoir, using TOUGH2 simulations. 38th Stanford Workshop on Geothermal Reservoir Engineering.

SCCER SoE

SWISS COMPETENCE CENTER for ENERGY RESEARCH
SUPPLY of ELECTRICITY

SCCER-SoE Annual Conference 2016

In cooperation with the CTI

Energy
Swiss Competence Centers for Energy Research

Schweizerische Eidgenossenschaft
Confédération suisse
Confederazione Svizzera
Confederaziun svizra

Swiss Confederation

Commission for Technology and Innovation CTI

Dynamics of boiling and condensation of saline fluids above magmatic intrusions

Samuel Scott, Thomas Driesner, Philipp Weis

Motivation

Subsurface magmatic intrusions emplaced in the upper crust provide heat that drives groundwater convection. Liquid-vapor coexistence in pure water terminates at the critical point (~22 MPa/374 °C), and systems containing dilute, meteoric-dominated fluids develop supercritical geothermal resources above intrusions, as long as host rocks remain permeable up to temperatures ≥450 °C (Scott et al., 2015). However, several active high-enthalpy geothermal systems, feature geothermal waters containing significant concentrations of dissolved salt. The behavior of saline water can be approximated by the system H_2O-NaCl, which shows liquid-vapor coexistence to temperatures and pressures far above the critical values of pure water (Sourirajan and Kennedy, 1962). Although economically-attractive supercritical geothermal resources have been discovered in systems with dilute thermal waters (Elders et al., 2014), it is presently unclear whether analogous resources form in saline systems, despite ongoing efforts to tap into such conditions in the Reykjanes geothermal system by the Iceland Deep Drilling Project (Fridleifsson et al., 2014)

Methods

The governing equations of mass and energy conservation for multi-phase flow of H_2O-NaCl fluids are solved using a continuum, porous media approach with a pressure-enthalpy-based formulation in a Control Volume-Finite Element Method numerical scheme using the Complex Systems Modeling Platform (CSMP++) (Weis et al., 2014). The simulations describe the instantaneous emplacement of an intrusion in host rocks with a permeability of 10^{-15} m^2 initially containing pore waters with seawater salinity. We choose this permeability value because previous studies have shown a host rock permeability near 10^{-15} m^2 is close to optimal for the formation of spatially extensive supercritical geothermal resources in pure water systems (Figure 1) [*Scott et al.*, 2015, 2016]. We performed exemplary simulations in which intrusion depth and brittle-ductile transition temperature are treated as variables.

Results

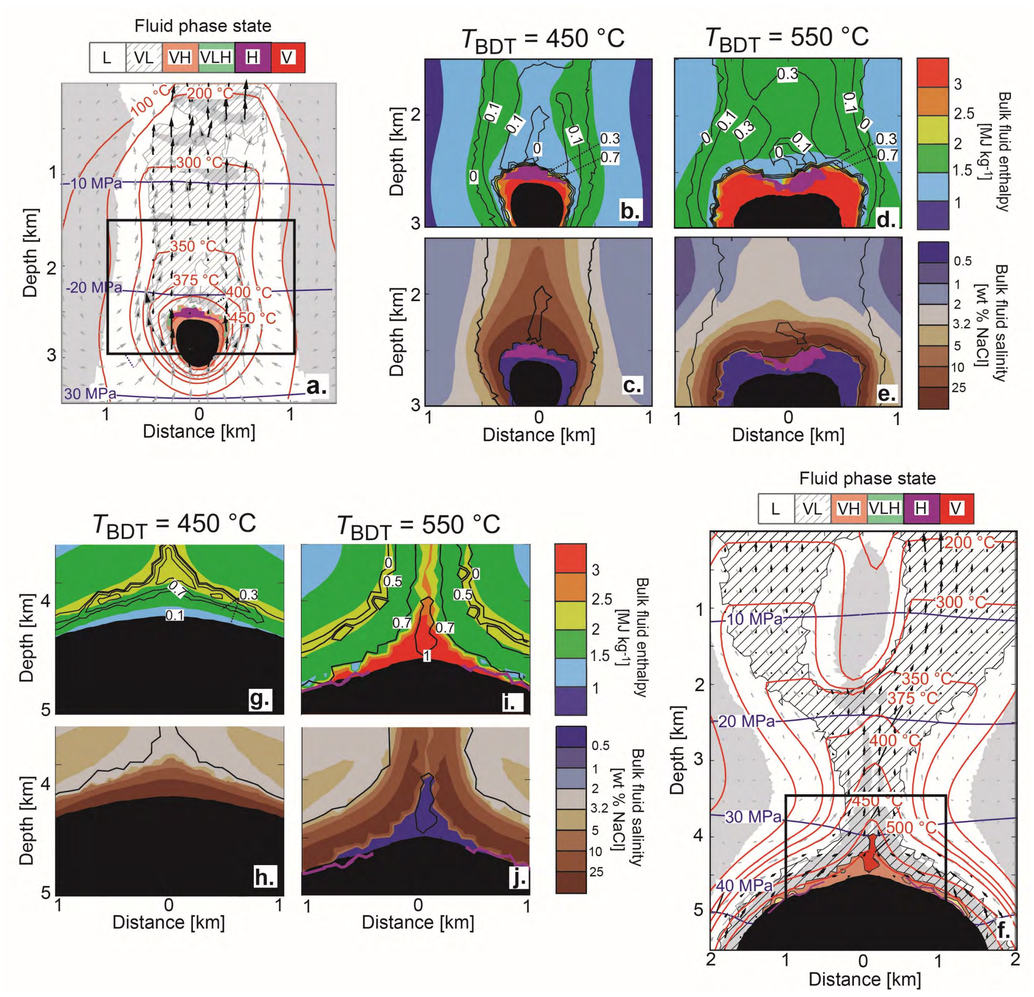

Figure 2. The thermal structure of saline geothermal systems above shallow (~2.5 km depth) or deep (~4.5 km) intrusions. showing fluid phase state, isotherms (red line), isobars (blue lines), and liquid pore velocity vectors (black). Areas where the vertical component of the liquid flow is oriented downwards are shown in grey. The location of the intrusion, defined by having a permeability <10^{-16} m^2, is shown in black. The area of the snapshots in b-e or g-j are shown by the black boxes in a and f, respectively. Snapshots show the evolution of fluid enthalpy and vapor saturation and salinity in systems with T_{BDT} of 450 °C (b,c,g,h) or 550 °C (d,e,i,j).

General Information

In contrast to the numerous efforts in Switzerland to study engineered geothermal systems (EGS), this study focuses on how to better exploit conventional high-enthalpy geothermal systems, typically located in volcanic settings. The COTHERM project (SNF Synergia) is a collaboration between the Paul Scherrer Institut and the University of Iceland. The project is nearing completion, and I have personally defended my PhD thesis. So far the major highlight of this work has been to present the first realistic simulations of supercritical geothermal resource formation near magmatic intrusions (Scott et al., 2015). Drilling into such resources could result in increased electricity generation by an order-of-magnitude per well compared to conventional wells drilled into such systems.

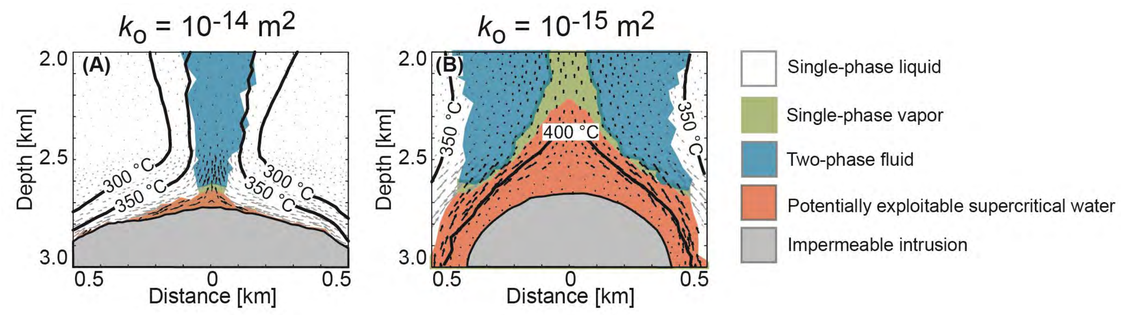

Figure 1. Supercritical geothermal resource formation depends on host rock permeability (after Scott et al., 2015). Fluid phase state distribution shown with colors (see legend) and temperature distribution shown with black lines. Snapshots under different conditions of host rock permeability (k_o) with a brittle-ductile transition temperature of 450 °C. We vary k_o from 10^{-14} m^2 (A) to 10^{-15} m^2 (B).

Discussion

Intrusion emplacement depth determines whether phase separation in the vicinity of an intrusion is dominantly carried out dominantly by boiling, as is the case for shallow intrusions, or condensation, which is dominant locally where single-phase vapor zones form above deep intrusions.

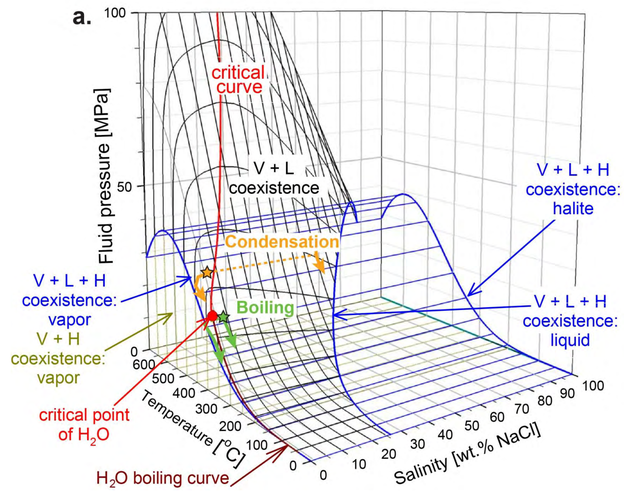

Figure 3. The effect of intrusion depth on patterns of phase separation above intrusions is illustrated schematically with the H_2O-NaCl phase diagram. Above shallow intrusions, phase separation by boiling occurs because fluid pressure near the intrusion is less than the critical pressure of seawater (~30 MPa). In the case of boiling, vapor bubbles nucleate out of a liquid-like fluid (green star, green lines). Seawater heated to 500 °C at ≥30 MPa intersects the vapor side of the VL surface (orange star) and a high-salinity liquid will condense upon phase separation of a vapor-like fluid (orange lines).

References

Driesner, T., and C. Heinrich (2007), The system H2O–NaCl. Part I: Correlation formulae for phase relations in temperature–pressure–composition space from 0 to 1000 °C, 0 to 5000 bar, and 0 to 1 XNaCl, Geochim. Cosmochim. Acta, 71(20), 4880–4901

Elders, W. A., G. Ó. Friðleifsson, and A. Albertsson (2014), Drilling into magma and the implications of the Iceland Deep Drilling Project (IDDP) for high-temperature geothermal systems worldwide, Geothermics, 49, 111–118

Scott, S., T. Driesner, and P. Weis (2015), Geologic controls on supercritical geothermal resources above magmatic intrusions., Nat. Commun., 6, 7837,

Scott, S., T. Driesner, and P. Weis (2016), The thermal structure and temporal evolution of high-enthalpy geothermal systems, Geothermics, 62, 33–47

Sourirajan, S., and G. C. Kennedy (1962), The System H_2O-NaCl at Elevated Temperatures and Pressures, Am. J. Sci., 260, 115–141.

Weis, P., T. Driesner, D. Coumou, and S. Geiger (2014), Hydrothermal, multiphase convection of H_2O-NaCl fluids from ambient to magmatic temperatures: a new numerical scheme and benchmarks for code comparison, Geofluids, 14(3), 347–371

SCCER SoE

SWISS COMPETENCE CENTER for ENERGY RESEARCH
SUPPLY of ELECTRICITY

SCCER-SoE Annual Conference 2016

In cooperation with the CTI

Energy
Swiss Competence Centers for Energy Research

Schweizerische Eidgenossenschaft
Confédération suisse
Confederazione Svizzera
Confederaziun svizra

Swiss Confederation

Commission for Technology and Innovation CTI

Reactive transport modelling of two-phase geothermal systems

A.Yapparova, D.A.Kulik, T.Driesner

Introduction

Magma-driven, high enthalpy geothermal systems are currently the only type of geothermal reservoirs that is routinely utilized for electrical power generation. The transient evolution of geochemical processes in the subsurface of these systems has remained elusive because direct observation is hampered by the extreme conditions in the boiling reservoir and the difficulties of undisturbed, in situ sampling in a producing geothermal field.
Numerical reactive transport simulation is, therefore, the tool of choice to study these processes and, combined with sampling, can lead to well-constrained models of chemical reservoir processes. In the context of the COTHERM2 project, we develop a novel reactive transport simulator that allows simulating reactive transport under boiling conditions on unstructured meshes.

Motivation: Geothermal systems

Chemical fluid-rock interaction an boiling modify the chemical composition of geothermal fluids and obscure their origin, which is of both academic and practical interest:

- Geologically constrained simulation allow unravelling the influence of these processes and quantifying the paths that fluids take, which will provide new insights into the mechanisms of heat and mass transfer
- The chemical composition of fluids controls factors such as corrosive behavior or heat extraction efficiency that operators like to control to optimize production

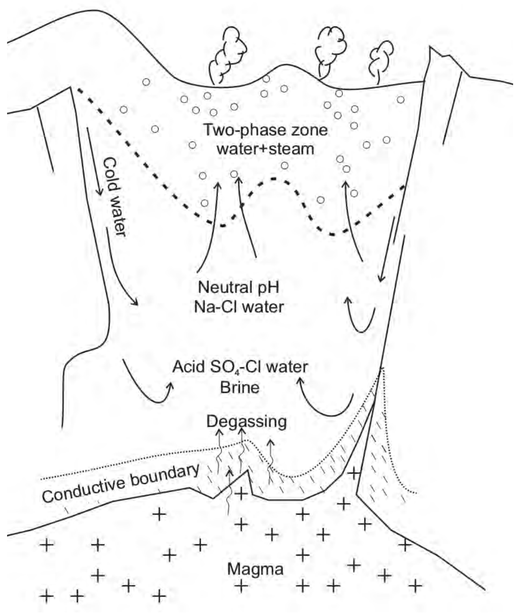

Figure 1. Schematic section of a volcanic geothermal system depicting the origin, interaction, and possible evolution of fluids. (Arnorsson et al., 2007)

Methods:
CSMP++GEM reactive transport code (Yapparova et al., 2016)

The combination of CSMP++ and GEMS3K provides a unique feature set. Namely, the combination of unstructured meshes with reactive transport in a boiling system has so far not been realized in any other tool and will allow us to perform simulations on "geologically realistic" geometries.

Methodological aspects include:

- Control volume finite element method (CVFEM) to solve PDEs for two-phase flow and heat transport in terms of pressure, enthalpy and salinity (Weis et al., 2014).
- Accurate thermodynamic representation of fluid properties – Equation of state for a H_2O-NaCl system (Driesner&Heinrich, 2007; Driesner, 2007)
- Chemical equilibrium calculations using the Gibbs energy minimisation method (GEM), implemented within the GEMS3K standalone library.
- Sequentital Non-Iterative Approach (SNIA) for transport-chemistry coupling allows fast reactive transport calculations (compared to SIA and fully implicit methods)
- Phase partitioning of gases (CO_2, H_2S, H_2, CH_4) is calculated in GEMS, additional constraints on the amount of vapor are provided from the CSMP++ part (Gibbs free energy on the boiling curve is the same for liquid water and vapor).
- Metastable water properties calculation was implemented in GEMS (liquid water in the vapor phase and steam in the liquid phase).
- Ideal mixture of gases with properties calculated from the Peng-Robinson equation of state is used.
- Liquid water and steam properties are taken from the HGK eos.

Example: Implementation of liquid-vapor partitioning during flow in a boiling system

1D simulation results: hot 300°C vapor is injected from the left into the 200°C warm liquid, a boiling zone develops in the middle part of the model, volatiles partition between the liquid and vapor phases. Aquifer fluid composition was calculated from the liquid and steam sample analysis of the K-14 well from the Krafla geothermal field.

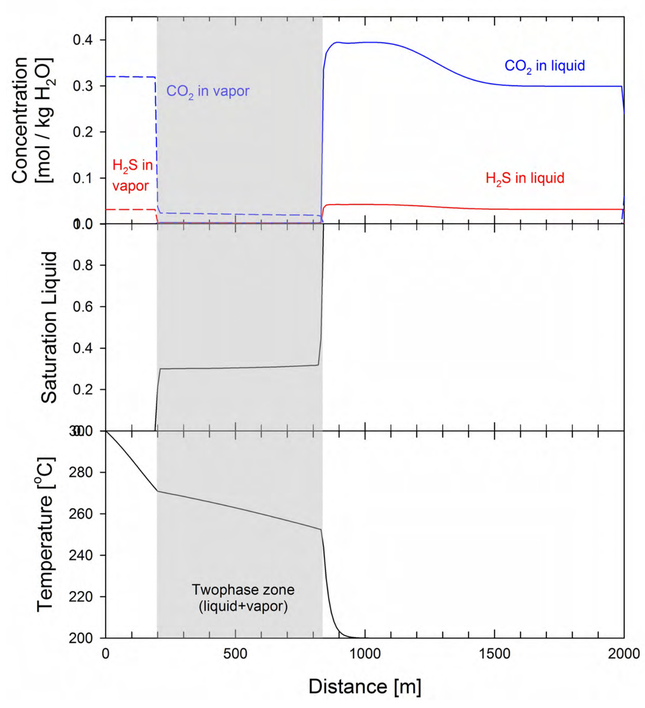

Figure 2. CO_2 and H_2S concentrations in the vapor and liquid phases, saturation of liquid and temperature distribution. Curve shapes reflect the competition of distribution coefficients and the masses of liquid and vapor along the flow path, including concentration changes due to condensation and boiling.

Discussion and outlook

Highlights
- Reactive transport code able to perform two phase flow simulations coupled with chemical reactions on unstructured grids
- Can be used for a quantitative assessment of the dynamic behavior of key chemical components in a Krafla-like geothermal system

Future work:
- Add fluid mineral interaction (basalt glass kinetics) and porosity/permeability evolution
- Calculate solution properties in GEM (at the moment effect of dissolved gases on density etc is not taken into account)
- Add other aqueous species, including Si(OH)4 and B(OH)3 using the Akinfeev-Diamond eos
- Peng-Robinson steam
- 2D simulations of high-enthalpy geothermal systems with chemical reactions
- Added value in view of the Energy Strategy 2050: adaptation to fractured reservoirs, i.e., for assessing effects in EGS-type systems

References

1. Arnorsson, S., Stefansson, A., Bjarnason, J.O., Fluid-Fluid interactions in geothermal systems. Reviews in Mineralogy & Geochemistry (2007) 65, 259-312.
2. Weis, P. and Driesner, T. and Coumou, D. and Geiger, S., Hydrothermal, multiphase convection of H2O-NaCl fluids from ambient to magmatic temperatures: a new numerical scheme and benchmarks for code comparison. Geofluids (2014) 14, 347–371
3. Driesner, T., Heinrich, C.A., The system H2O–NaCl. Part I: Correlation formulae for phase relations in temperature–pressure–composition space from 0 to 1000 °C, 0 to 5000 bar, and 0 to 1 X_NaCl. Geochimica et Cosmochimica Acta (2007) 71, 4880 - 4901
4. Driesner, T., The system H2O–NaCl. Part II: Correlations for molar volume, enthalpy, and isobaric heat capacity from 0 to 1000 °C, 1 to 5000 bar, and 0 to 1 X_NaCl. Geochimica et Cosmochimica Acta (2007) 71, 4902 - 4919
5. Yapparova A., Gabellone, T., Whitaker, F., Kulik, D.A., Matthai, S., Reactive transport modelling of dolomitisation using the new CSMP+ +GEM coupled code: governing equations, solution method and benchmarking results (submitted)

SCCER SoE

SWISS COMPETENCE CENTER for ENERGY RESEARCH
SUPPLY of ELECTRICITY

SCCER-SoE Annual Conference 2016

In cooperation with the CTI
Energy
Swiss Competence Centers for Energy Research

COTHERM – Seismic Characterization of Fractured Magmatic Geothermal Reservoirs

Melchior Grab, Hansruedi Maurer, Stewart Greenhalgh — *Institute of Geophysics, ETH Zürich*

Motivation:

- The main task in seismic interpretation is to link the measured quantities (e.g. seismic velocities) with the features of interest (energetic state of the pore fluid and presence of permeable structures).
- Typical rocks in magmatic geothermal systems are highly impermeable, why fluid flow is expected to take place in large scale fracture networks.
- Studying seismic properties of geothermal reservoirs requires up-scaling from laboratory scales (small intact rock samples) to field scales (large jointed rock volumes) using numerical modelling techniques.

Modelling Techniques:

Seismic properties of intact rock were modelled using the numerical modeling technique proposed by Quintal et al. (e.g. 2011). It is based on Biot's theory (1941) and the principle of conservation of linear momentum:

$$\nabla \cdot \sigma = 0,$$

where the components of the stress tensor σ are defined (in 2-D) by

$$\sigma_{ij} = 2G_d\varepsilon_{ij} + \lambda\left(\varepsilon_{11}+\varepsilon_{22}\right)\delta_{ij} - \alpha P_{pore}\delta_{ij},$$

with ε being the strain tensor, $\alpha = 1\text{-}K_d/K_s$, $\lambda = K_d - 2/3G_d$, and δ_{ij} being the Kronecker Delta. This is equivalent to Hook's law, extended by an additional term incorporating the stiffening of the rock in response to a pore pressure P_{pore}. It is linked to wave induced fluid flow by Darcy's law, combined with the conservation of fluid mass, yielding the frequency dependent relation

$$-k/\eta_f \nabla^2 P_{pore} + i\omega\alpha\left(\varepsilon_{11}+\varepsilon_{22}\right) + i\omega M P_{pore} = 0,$$

given in the space-frequency domain. Quantity η_f is the fluid viscosity, and $M = \phi/K_f - (\alpha-\phi)/K_s$, with K_f being the fluid incompressibility.
Solving for the strain ε responding to a given stress σ, first requires the determination of the hydro-mechanical properties of fractures and the surrounding intact rock. This comprises the following sets of parameters:

	Intact rock:	Fractures:
Dry frame bulk modulus:	$\hat{K}_d$	$\tilde{K}_d$
Dry frame shear modulus:	$\hat{G}_d$	$\tilde{G}_d$
Solid phase bulk modulus:	$\hat{K}_s$	$\hat{K}_s = \tilde{K}_s$
Effective porosity:	$\hat{\phi}$	$\tilde{\phi} \rightarrow 1$
Dry bulk density:	$\hat{\rho}_b$	$\tilde{\rho}_b$
Hydraulic permeability:	$\hat{k}$	$\tilde{k}$

Intact rock properties:

- Intact rock properties were documented in numerous laboratory studies published over the last decades. A compilation of their results is shown in Figure 1.
- Considering the large diversity of rock types being present in magmatic geothermal systems (Figure 1-a), values vary over wide ranges.
- For the numerical modelling, we extracted four sets of parameters, shown by the colour-coded dots in Figure 1, with values listed in Table 1.

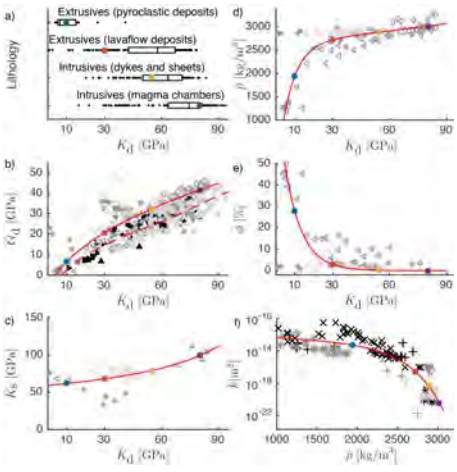

Figure 1: Intact rock properties, taken from various studies in the rock physics literature.

Table 1: Intact rock properties for the four lithologies (A-D) given in Figure 1-a.

	Model A	Model B	Model C	Model D
$\hat{K}_d$[GPa]	10	30	55	80
$\hat{G}_d$[GPa]	7	21	32	42
$\hat{K}_s$[GPa]	62	68	79	99
$\hat{\phi}$[%]	27.44	2.89	0.17	0.01
$\hat{k}$[m²]	5.10e-14	2.55e-17	3.79e-19	3.72e-21

Fracture Properties:

- $\tilde{K}_d$ and $\tilde{G}_d$ of fractures were obtained by cross-fitting the response of a numerical model containing non-interacting fractures (Figure 2-a) with the semi-analytical effective medium theory for fractures of idealized geometry (Figure 2-b).
- The hydraulic permeability was deduced from the cubic law (e.g. Barton et al. 1985)

$$\hat{k} = e_h^{\,2}/12 \quad \text{with} \quad e_h = \mathrm{JRC}^{2.5}/\left(h/e_h\right)^2 \; [\mu\mathrm{m}]$$

where h is the fracture aperture and JRC the joint roughness coefficient.
- The porosity was set to a high value, assuming the fractures being free of fault gauge, and the solid phase bulk modulus is identical with the one of intact rock, assuming the mineralogy being homogeneous across the entire jointed rock mass.

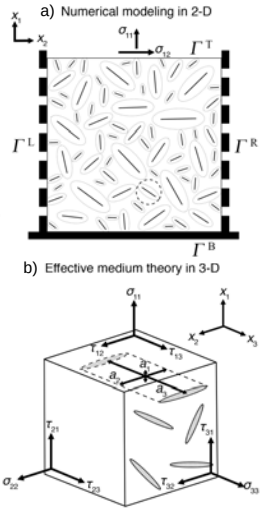

Figure 2: Concept of numerical modelling (a) and of the effective medium theory (b).

Table 2: Fracture properties for the four lithologies (A-D, see Figure 1-a).

	Model A	Model B	Model C	Model D
$\tilde{K}_d$[MPa]	2.8 - 5.8	9.3 - 16.2	12.8 - 26.7	17.8 - 34.6
$\tilde{G}_d$[MPa]	1.7 - 3.7	5.9 - 10.1	8.0 - 16.8	11.0 - 21.2
$\tilde{K}_s$[GPa]	62	68	79	99
$\tilde{\phi}$[%]	90	90	90	90
$\tilde{k}$[m²]	2.81e-09 - 4.03e-07	2.81e-09 - 4.03e-07	2.81e-09 - 4.03e-07	2.81e-09 - 4.03e-07

Example: Seismic properties of fractured rock:

- Seismic properties of a fractured rock model (Geometry in Figure 3) were calculated using the parameters listed in Table 1 and 2.
- From numerical modelling we obtained the plane wave moduli

$$M_c(\omega) = \sigma_{11}/\varepsilon_{11}$$

and shear wave moduli

$$G_c(\omega) = \tfrac{1}{2}\sigma_{12}/\varepsilon_{12}$$

- These are complex, frequency dependent quantities, allowing calculating the seismic velocities by

$$V_P(\omega) = \mathrm{Re}\left(\sqrt{\rho_b/M_c}\right)^{-1}$$

$$V_S(\omega) = \mathrm{Re}\left(\sqrt{\rho_b/G_c}\right)^{-1}$$

- The seismic attenuation factors are defined by

$$Q_P^{-1}(\omega) = \mathrm{Im}\left(M_c\right)/\mathrm{Re}\left(M_c\right)$$

$$Q_S^{-1}(\omega) = \mathrm{Im}\left(G_c\right)/\mathrm{Re}\left(G_c\right)$$

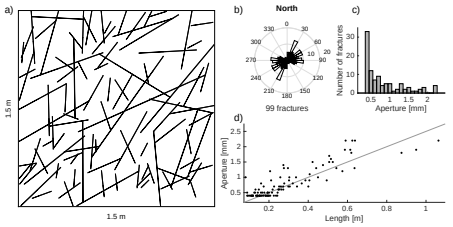

Figure 3: Fractured rock model (a) and geometry statistics (b).

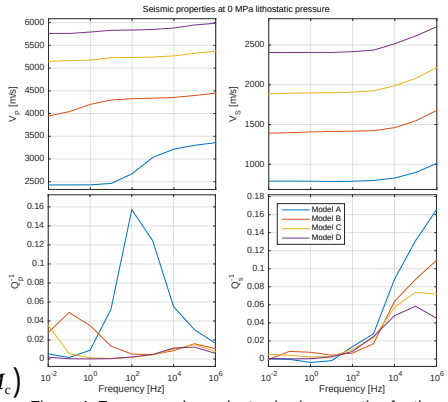

Figure 4: Frequency dependent seismic properties for the fractured rock shown in Figure 3.

Acknowledgements:

We thank Eva Caspari and Beatriz Quintal from the Institute of Earth Science, University of Lausanne, for the close cooperation.

References:

Barton, N., Bandis, S., & Bakhtar, K. (1985). Strength, deformation and conductivity coupling of rock joints. In *International Journal of Rock Mechanics and Mining Sciences & Geomechanics Abstracts* (Vol. 22, No. 3)

Biot, M. A. (1941). General theory of three-dimensional consolidation. *Journal of applied physics*, *12*(2), 155-164.

Quintal, B., Steeb, H., Frehner, M., & Schmalholz, S. M. (2011). Quasi-static finite element modeling of seismic attenuation and dispersion due to wave-induced fluid flow in poroelastic media. *Journal of Geophysical Research: Solid Earth*, *116*(B1).